https://doi.org/10.5194/gchron-2024-34
Preprint. Discussion started: 9 December 2024


# Paired $^{14}C$-$^{10}Be$ exposure ages from Mount Murphy, West Antarctica: Implications for accurate and precise deglacial chronologies

Jonathan R. Adams[1,2], Dylan H. Rood[1], Klaus Wilcken[3], Stephen J. Roberts[2] and Joanne S. Johnson[2]

[1]Department of Earth Science & Engineering, Imperial College London, Exhibition Road, London, SW7 2AZ, UK

[2]British Antarctic Survey, High Cross, Madingley Road, Cambridge, CB3 0ET, UK

[3]Australian Nuclear Science and Technology Organization, Lucas Heights, NSW 2234, Australia

*Correspondence to*: Jonathan R. Adams (j.adams19@imperial .ac.uk)

**Abstract.** Cosmogenic-nuclide surface exposure ages provide empirical data for testing the accuracy of models simulating the timing and pace of ice sheet response to a warming climate. Increasing emphasis is being placed on obtaining exposure ages that both accurately constrain Holocene deglaciation and are precise enough to capture ice sheet change at the sub-millennial scale. However, the accuracy of Holocene deglacial chronologies can be compromised by nuclide inheritance when measuring longer-lived nuclides, such as $^{10}Be$. Short-lived in situ-produced $^{14}C$ is unique because it is largely insensitive to nuclide inheritance pre-dating the last glacial maximum (LGM), and when combined with longer-lived nuclides can be used to constrain complex ice sheet histories over Holocene timescales. Here, we present new in situ $^{14}C$ exposure ages from Mt Murphy, West Antarctica. Many of the new in situ $^{14}C$ ages are inconsistent with published $^{10}Be$ ages, suggesting samples collected from the same elevation above the modern ice were exposed at different times. We investigate potential explanations for such conflicting exposure histories by analysing paired $^{14}C$-$^{10}Be$ data of Holocene age presently archived in the informal cosmogenic-nuclide exposure-age database (ICE-D, https://version2.ice-d.org/). Our analysis reveal that neither geologic sources of uncertainty due to variations in geologic setting nor modelled scenarios of subsurface nuclide production explain conflicting paired $^{14}C$-$^{10}Be$ exposure ages observed at Mt Murphy. Furthermore, we observe that repeat in situ $^{14}C$ concentrations measured in 15 of 31 samples do not replicate within their nominal 6 % (2σ) analytical uncertainty and identify ~ 2 kyr of excess unquantified scatter from Mt Murphy in situ $^{14}C$ exposure ages. Taken together, these results suggest analytical uncertainty for in situ $^{14}C$ measurements may currently be underestimated. We provide recommendations for improving measurement precision that will benefit future Holocene deglaciation studies including analysis and publication of more replicate measurements, and the continuation of efforts to quantify and minimise sources of scatter in blank measurements.

https://doi.org/10.5194/gchron-2024-34
Preprint. Discussion started: 9 December 2024


## 1. Introduction

Increasing emphasis is being placed on glacial chronologies that both constrain the timing of ice surface change during the Holocene epoch and provide validation for model simulations at sub-millennial scale resolution (Hippe, 2017; Nichols et al., 2019; Jones et al., 2022; Johnson et al., 2022). To provide Holocene deglacial chronologies for ice sheet models at sub-millennial scale resolution, cosmogenic radionuclide (e.g., in situ $^{14}$C and $^{10}$Be) exposure ages must both be accurate and precise. Accurately determining a Holocene exposure age relies on the assumption that the sample being dated is free from nuclides accumulated during periods of surface exposure that pre-date the LGM (Balco, 2011). The prevalence of cold-based ice and subsequent lack of basal erosion, however, often leads to longer-lived nuclides such as $^{10}$Be (half-life; 1.387 Myr) persisting over multiple glacial cycles impacting the accuracy of deglacial chronologies (Balco, 2011; Hein et al., 2014). The short half-life of in situ $^{14}$C of (5700 ± 30 years), results in the total inventory of in situ $^{14}$C in a sample decaying to below detectable levels in ~30 kyr, making in situ $^{14}$C largely (and uniquely) insensitive to pre-LGM exposure. Following efforts to develop and improve in situ $^{14}$C extraction (Lifton, 1997; Lifton et al., 2001, 2015b; Hippe et al., 2009, 2013; Fülöp et al., 2010, 2015; Goehring et al., 2014, 2019a; Lamp et al., 2019) in situ $^{14}$C, has been increasingly applied to accurately determine Holocene exposure ages where $^{10}$Be inheritance is known or suspected (White et al., 2011; Briner et al., 2014; Nichols et al., 2019). Combining analyses of the short-lived in situ $^{14}$C nuclide with longer-lived $^{10}$Be (or $^{26}$Al) presents a valuable approach to reveal and quantify complex exposure histories (Hippe, 2017). However, there is added value in this approach if measurement precision of both nuclides is sufficient to resolve past ice sheet behaviour at the sub-millennial timescale, which is necessary to distinguish early-mid Holocene retreat of the West Antarctic Ice Sheet from possible late Holocene ice sheet readvance for which there is emerging evidence (Kingslake et al., 2018; Venturelli et al., 2020; Balco et al., 2023; Venturelli et al., 2023).

In this study, we measured in situ $^{14}$C in a selection of samples from Mt Murphy, a volcanic edifice adjacent to Thwaites Glacier in the Amundsen Sea Embayment (Fig. 1a) to investigate if published $^{10}$Be ages (Johnson et al., 2020; Adams et al., 2022) contained small amounts of nuclide inheritance. However, new in situ $^{14}$C ages suggest two conflicting exposure histories at Mount Murphy. Some paired in situ $^{14}$C-$^{10}$Be ages from the same sample are concordant (paired $^{14}$C-$^{10}$Be ages agree within uncertainty), indicating the sample experienced a simple post-LGM exposure history. Other samples returned discordant exposure ages (paired $^{14}$C-$^{10}$Be ages did not overlap within analytical uncertainty) indicating that, since post-LGM exposure, a sample experienced burial or there were changes in the nuclide production rate (Balco et al., 2019). Discordant in situ $^{14}$C-$^{10}$Be exposure ages have previously permitted detection of considerable inheritance in $^{10}$Be nuclide concentrations ranging from 10s–100s kyr (e.g., Nichols et al., 2019). However, the paired $^{14}$C-$^{10}$Be data from Mt Murphy presented here are distinct because i) both new in situ $^{14}$C and $^{10}$Be exposure ages are younger than the LGM and ii) replicate in situ $^{14}$C ages presented in this study do not reproduce within currently stated uncertainties to such an extent they suggest conflicting mid and late-Holocene exposure histories, which is problematic given the need for exposure age chronologies capable of reconstructing post-LGM ice sheet change on sub-millennial timescales.

Here, we describe an investigation into potential explanations for co-existing concordant and discordant paired $^{14}$C-$^{10}$Be Holocene exposure ages observed at Mt Murphy. We do this by revisiting the data of Johnson et al., 2020 and Adams et al., (2022),

https://doi.org/10.5194/gchron-2024-34
Preprint. Discussion started: 9 December 2024


and performing a more in-depth examination of sources of uncertainty associated with both in situ $^{14}C$ and $^{10}Be$ exposure ages. First, we present a new in situ $^{14}C$ dataset from Mt Murphy (paired with previously published $^{10}Be$ measurements) (Fig. 1a) and assess the accuracy and reproducibility of this new dataset. We then contextualise the new Mt Murphy dataset by analysing available $^{14}C$-$^{10}Be$ paired exposure age data that is of Holocene age (< ~ 11.7 ka) from Antarctica (Fig. 1b) and globally (Fig. 1c). These paired $^{14}C$-$^{10}Be$ data are primarily sourced from the Informal Cosmogenic-nuclide Exposure age Database (ICE-D; Balco, 2020b) (https://version2.ice-d.org/). Through this work we aim to use the new and existing paired $^{14}C$-$^{10}Be$ exposure age data to assess, progress and identify steps the community could take to consistently produce robust Holocene glacial chronologies.

### 1.1 Sources of uncertainty that impact in situ $^{14}C$ and $^{10}Be$ exposure ages

To provide additional context for our results and discussion, we first outline sources of uncertainty that need to be accounted for when calculating in situ $^{14}C$ and $^{10}Be$ exposure ages. The source of uncertainty over which cosmogenic nuclide practitioners have the least control is geologic uncertainty, inherent in a sample from its time of collection in the field and rooted in the limited knowledge we have of a samples true exposure history and any processes that may have modified production of nuclides following exposure (Dunai, 2010). The two main sources of geologic uncertainty are nuclide inheritance (described above) and post depositional disturbance caused by shielding, erosion, and/or rolling of a sample (Gosse and Phillips, 2001; Balco, 2011). Steps taken to reduce geologic uncertainty include a robust and detailed geologic interpretation of deposits or depositional features being dated (Balco, 2011) and statistical techniques (e.g., Johnson et al., 2014; Heyman et al., 2016). Comprehensive summaries of geologic uncertainty and previous and ongoing efforts to quantify it can be found in Balco et al., (2011, 2020b).

The second major source of uncertainty comes from our ability to measure the nuclide concentration accurately and precisely within a sample. A crucial distinction, and source of potential confusion, is that we commonly refer to the accuracy and precision associated with determining the concentration of a sample (Jull et al., 2015), which itself forms a component of the total uncertainty of an exposure age (Balco, 2020a). Data producers make efforts to minimise contributions of measurement uncertainty from two main sources: uncertainties introduced during sample preparation and sample measurement by accelerator mass spectrometry (AMS). Measurement of the cosmogenic nuclide $^{10}Be$ is now relatively well-established and routine following incremental efforts to reduce sources of laboratory sample preparation uncertainty (Kohl and Nishiizumi, 1992; Corbett et al., 2016, 2022) and improve AMS performance (Rood et al., 2010, 2013; Merchel et al., 2012; Wilcken et al., 2022). These efforts have resulted in $^{10}Be$ measurement precision on typical quartz interlaboratory comparison materials (e.g., CRONUS-A, CoQtz-N) of between ~2–4 % (Jull et al., 2015; Phillips et al., 2016a; Binnie et al., 2019).

Measurement of the isotope $^{14}C$ (radiocarbon) by AMS is also routine with precision consistently reported in the range of 2–3% (Roberts et al., 2010; Scott et al., 2017; Aerts-Bijma et al., 2021). In situ $^{14}C$ measurement from quartz is, however, less mature, in part due to the significant challenges associated with its sample preparation and extraction (Lifton et al., 2001; Hippe et al., 2009; Fülöp et al., 2010; Goehring et al., 2014; Lifton, 1997). Laboratory intercomparison studies of CRONUS-A indicate the coefficient of variation (CoV) of in situ $^{14}C$ is currently in the range of 6–8 %, double the values reported for $^{10}Be$ (Phillips et al., 2016a). Recent improvements to the in situ $^{14}C$ extraction process include identification of potential contaminant “dead” carbon

https://doi.org/10.5194/gchron-2024-34
Preprint. Discussion started: 9 December 2024


sources during quartz purification (Nichols and Goehring, 2019), and automation of $^{14}C$ extraction lines to reduce risk of atmospheric $^{14}C$ contamination and potential for human error (e.g., Lifton et al., 2015, 2023; Goehring et al., 2019b; Lupker et al., 2019). Potential refinement of the in situ $^{14}C$ combustion step is also being explored (Lifton et al., 2023) as well as omitting graphitisation in favour of directly analysing in situ $^{14}C$ using gas source AMS (e.g., Lamp et al., 2019).

The final major source of uncertainty comes from transforming a measured nuclide concentration into an exposure age, which requires estimating the production rate due to secondary spallation reactions, which accounts for the majority of surface production (Dunai, 2010), and by muons (Balco, 2017). Production rate uncertainties have been incrementally reduced by improvements in scaling models, especially using more recent models based on particle-physics simulations (Lifton et al., 2014; Argento et al., 2015a, b). Estimates of the $^{10}Be$ production rate uncertainty from spallation are currently in the range of 6 % (Borchers et al., 2016; Marrero et al., 2016). However, in the case of in situ $^{14}C$ a spallogenic production rate uncertainty could not be fitted to the data because of the large scatter in measured in situ $^{14}C$ concentrations (in excess of an assumed 7.3 % measurement uncertainty) observed at in situ $^{14}C$ calibration sites (Borchers et al., 2016).

Muons account for a smaller proportion of total cosmogenic nuclide production at the surface, but this quantity differs for $^{10}Be$ and in situ $^{14}C$. For $^{10}Be$ the proportion of cosmogenic nuclide production by muons at the surface is between 1.5–2 %. In the case of in situ $^{14}C$ ~ 20 % of surface production is estimated to be from muons (Lupker et al., 2015). The total uncertainty on computing a production rate by muons at an arbitrary location has been estimated between 10–25 % (Balco, 2017). This results in a total maximum scaling uncertainty of only 0.5 % for estimating $^{10}Be$ production by muons. However, for in situ $^{14}C$, the same 10–25 % uncertainty on calculating production by muons equates to a 5 % uncertainty on the total surface production rate estimate (Balco, 2017). Because the in situ $^{14}C$ production rate by muons as a proportion of total surface production is an order of magnitude higher than for $^{10}Be$, it results in the $^{14}C$-$^{10}Be$ production ratio increasing with depth below the surface (Hippe, 2017). A sample that is buried under a thin layer of rock, ice, till or other material, and then rapidly exhumed by plucking can, therefore, exhibit seemingly "impermissible" paired $^{14}C$-$^{10}Be$ concentrations due to differences in the $^{14}C$-$^{10}Be$ total production ratio at the surface versus at depth (Hippe, 2017; Rand and Goehring, 2019).

In summary, sources of geologic, sample preparation and exposure age calculation uncertainty impact the accuracy and precision of Holocene deglaciation chronologies. An increase in paired $^{14}C$-$^{10}Be$ measurements in the recent ~ 5 years, driven by greater $^{14}C$ extraction throughput (Lifton et al., 2015b; Goehring et al., 2019a) provide many new data to make an assessment of the application of both nuclides and investigate sources of uncertainty, particularly of in situ $^{14}C$. In the following sections, we investigate the cause of concordant and discordant paired in situ $^{14}C$-$^{10}Be$ exposure ages at Mt Murphy and potential causes for the large amounts of scatter in reported in situ $^{14}C$ measurements using both the new in situ $^{14}C$ data from Mt Murphy and existing paired in situ $^{14}C$-$^{10}Be$ data extracted from ICE-D.

https://doi.org/10.5194/gchron-2024-34
Preprint. Discussion started: 9 December 2024


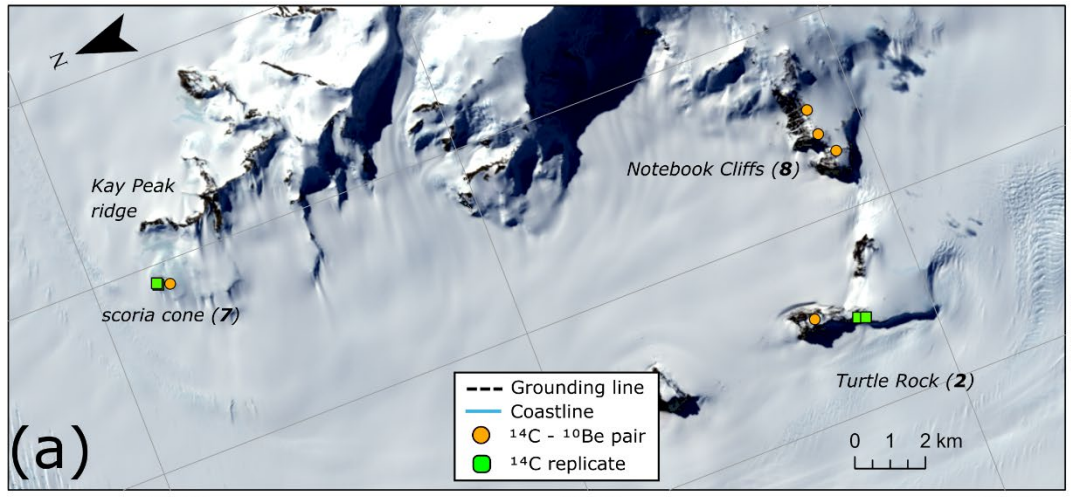


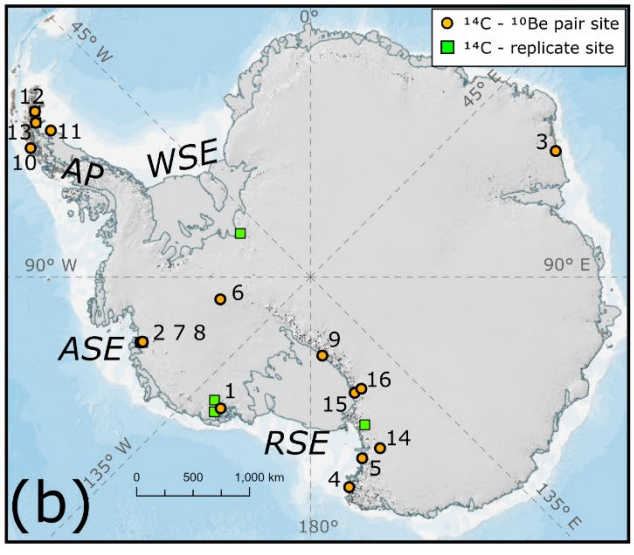


**Panel b: Pair Sites (1 - 16)**

1. Mt. Rea (Stone et al., 2003)
2. Turtle Rock (Johnson et al., 2020)
3. North Masson Range (White et al., (2011)
4. Shark Fin Nunatak (Balco et al., 2019)
5. MZS (Goehring et al., 2019)
6. Whitmore Mts. (Spector et al., 2019)
7. scoria cone (Adams et al., 2022)
8. Notebook Cliffs (Johnson et al., 2020)
9. Beardmore Gl. (Spector et al., 2017)
10. Cape Marsh (Jeong et al., 2018)
11. Cape Framnes (Jeong et al., 2018)
12. Sjögren Gl. (Balco & Schaefer, 2013)
13. Drygalski Gl. (Balco & Schaefer, 2013)
14. Mt. Kring (Stutz et al., 2021)
15. Diamond Hill (Hillebrand et al., 2021)
16. Danum Plat. (Hillebrand et al., 2021)

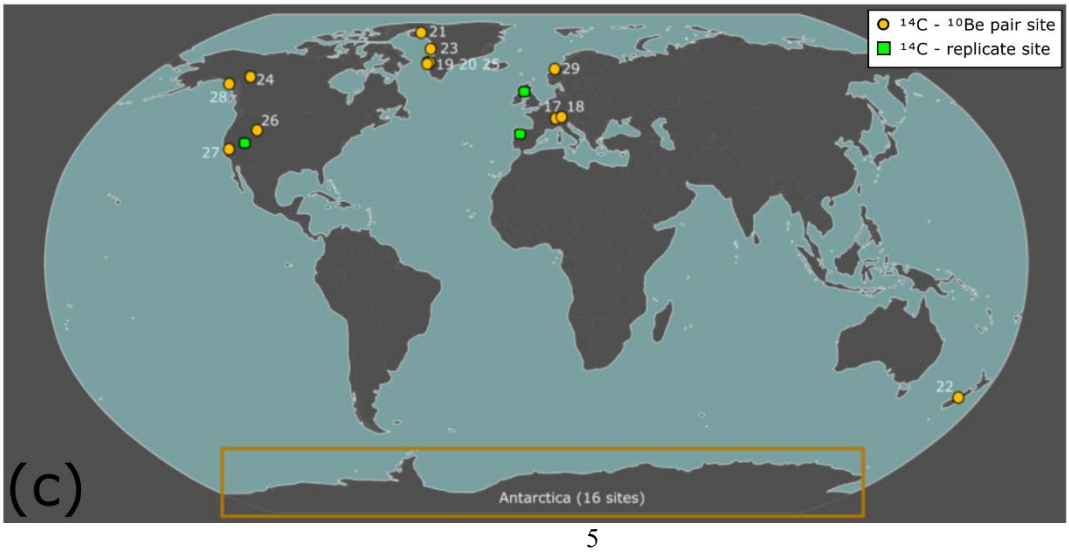

https://doi.org/10.5194/gchron-2024-34
Preprint. Discussion started: 9 December 2024


**Figure 1 (overleaf): Panel (a)** a Landsat-9 satellite image of the Turtle Rock, scoria cone and Notebook Cliffs sites at Mt Murphy showing locations of samples with new in situ $^{14}C$ exposure ages and previously published $^{10}Be$ exposure ages. Grounding line position uses data from (Milillo et al., 2022) and Antarctic Coastline is from version 7.7 of the Antarctic Digital Database. **Panel (b)** shows Antarctic and **Panel (c)** global site locations of paired $^{14}C$-$^{10}Be$ ages (sites 1-29) where both: i) apparent $^{10}Be$ exposure ages are < 4x older than apparent $^{14}C$ exposure ages ii) $^{10}Be$ exposure ages are of Holocene age (< 11.7 ka). Site numbering uses the order of the specific site ID (lowest to highest) that locations have been assigned in ICE-D (Balco, 2020b). **Panel (b)** Antarctic paired $^{14}C$-$^{10}Be$ site locations (1-16) are specified in an inset figure key. Panel **(b)** abbreviations indicate the Antarctic Peninsula (***AP***), Amundsen Sea Embayment (***ASE)***, Ross Sea embayment (***RSE***) and Weddell Sea embayment (***WSE***). Details of global site locations (17-29) displayed in **Panel (c)** are specified in Results, Table 2. Green squares in Panel **c)** indicate locations where multiple in situ $^{14}C$ measurements have been made on the same sample including Lake Bonneville, Utah, Northwest Highlands, Scotland and Leymon High, Northwest Spain (see Fig. 9, Table S3). Note in **Panel (a)** the corresponding site number from the global site index (**1-29**) is specified in bold italics along with the name of the sample site, e.g., Turtle Rock (***2***). Note in **panel (b)** paired in situ $^{14}C$-$^{10}Be$ sites 2, 7, 11 and 13 also contain replicate in situ $^{14}C$ measurements but only the paired $^{14}C$-$^{10}Be$ symbol (orange circle) is displayed.

## 2 Methods

### 2.1 In situ $^{14}C$ analysis of Mt Murphy samples

We selected nine samples from Mt Murphy (Table 1) for in situ $^{14}C$ analyses that had previously been measured for $^{10}Be$ (Johnson et al., 2020; Adams et al., 2022). The vertical thinning history derived from these $^{10}Be$ analyses implies the latest period of exposure of those samples occurred during the Holocene. We ensured that paired $^{10}Be$ and $^{14}C$ exposure ages cover a wide elevation range by selecting samples from three different locations around the Mt Murphy massif (Notebook Cliffs, samples collected from 893–834 m a. s. l., Turtle Rock, 700–441 m a. s. l., and a scoria cone adjacent to Kay Peak, 240–180 m a. s. l.). A general geological description of these sites (see Fig. 1a) is provided in Johnson et al (2020) and Adams et al., 2022. Geomorphic descriptions and supporting information of the nine samples with paired $^{14}C$-$^{10}Be$ measurements are provided in Supplement S1,and Table S2.

We selected five of the nine samples: CIN-108, CIN-112, TUR-117, TUR-132 and NOT-103, for repeat in situ $^{14}C$ measurements. The in situ $^{14}C$ extraction of NOT-103 failed, therefore, only four in situ $^{14}C$ measurements were repeated. We performed quartz mineral separation for in situ $^{14}C$ samples at Imperial College London largely following Corbett et al., (2016) We omitted the froth flotation step (used to separate feldspars and quartz) following recommendations made by Nichols and Goehring (2019), and instead performed 3 x 1 % $HF/HNO_3$ etches to isolate the quartz. Quartz purity was determined using Inductively Coupled Plasma Optical Emission Spectrometry (ICP-OES), after which ~10 g of purified quartz from each sample was sent to Tulane University (New Orleans, USA) for in situ $^{14}C$ extraction. Extraction of in-situ $^{14}C$ (n = 9) was performed using the fully automated Carbon Extraction and Graphitisation System (CEGS) at Tulane University following the methods of Goehring et al., (2019a). The quartz sample was fused with lithium metaborate ($LiBO_2$) flux to ensure total sample melt <1300 °C and complete liberation of in-situ $^{14}C$ (Lifton et al., 2001). First quartz was step heated at 500°C for 1 hour to remove atmospheric $^{14}C$ before being combusted at 1100°C for 3 hours to liberate in situ $^{14}C$ (in the form of $CO_2$). Liberated $CO_2$ was cryogenically purified before being collected in a measurement chamber, quantified monometrically and diluted with $^{14}C$-free $CO_2$ to ensure a measurable sample size (Goehring et al., 2019a). $CO_2$ was graphitized using standard $H_2$ reduction methods over an Fe catalyst (Slota et al., 1987).

https://doi.org/10.5194/gchron-2024-34
Preprint. Discussion started: 9 December 2024


Several changes were made to the configuration of the extraction line prior to the replicate measurements (n = 4). Alterations to the line included a new coil trap, which changes how gas is extracted and trapped following combustion (Lifton et al., 2023) and the introduction of a new mullite tube for $^{14}C$ extraction due to failure of the previous tube. Mullite tubes often undergo a "break in" period, during which initial $^{14}C$ blanks are higher but often fall with continued use (Goehring et al., 2014, 2019a; Pigati et al., 2010).

$^{14}C/^{12}C$ isotope ratios were measured by accelerator mass spectrometry at the National Ocean Sciences Accelerator Mass Spectrometry Facility (NOSAMS) (Woods Hole, USA) using the methods described in Longworth et al., (2015) Stable isotope ($\delta^{13}C$) analysis was undertaken at the University of California, Davis Stable Isotope Facility. Data reduction (to convert $^{14}C/^{12}C$ ratios to $^{14}C/C_{total}$) followed methods outlined in Hippe and Lifton (2014) which account for the specific differences of $^{14}C$ production within a mineral lattice compared to $^{14}C$ incorporation into organic material. The long-term average $^{14}C$ blank used to correct the initial measurements of in situ $^{14}C$ (n = 9) is 4.53 ± 0.24 x $10^4$ atoms $g^{-1}$. For replicate measurements (n = 4), a higher short-term average $^{14}C$ blank of 7.14 ± 0.30 x $10^4$ $^{14}C$ atoms $g^{-1}$ is used (Table S1).

We assigned a 6 % (1σ) uncertainty to each in situ $^{14}C$ measurement concentration reported by AMS before calculating exposure ages. The 6 % uncertainty follows recommendations of Hippe (2017) and others that reporting of in situ $^{14}C$ data should fully propagate uncertainty relating to intra-laboratory scatter as well as AMS measurement errors and errors relating to blank correction. The 6 % uncertainty exceeds the reported analytical uncertainty for all in situ $^{14}C$ measurements made for this study and reflects the repeatability of measurements of CRONUS-A extracted at Tulane. This 6% uncertainty has been adopted by studies where in situ $^{14}C$ extraction was carried out at Tulane University, e.g., Nichols et al., (2019). The in situ $^{14}C$ concentration of CRONUS-A extracted at Tulane has a long-term value of 6.12 ± 0.32 x $10^5$ (n = 10) (Goehring et al., 2019a).

We calculated exposure ages for the new in situ $^{14}C$ measurements, as well as for the published $^{10}Be$ measurements using version 3 of the online calculators (https://hess.ess.washington.edu/math/v3/v3_age_in.html) with the "LSDn" production rate scaling method for neutrons, protons, and muons (following Lifton et al. (2014) and summarised in Balco (2017)) and the primary production rate calibration data set of Borchers et al. (2016). When comparing in situ $^{14}C$ and $^{10}Be$ exposure ages at Mt Murphy, we used the external uncertainty, which includes the 6 % 1σ measurement uncertainty propagated in quadrature with the production rate and scaling scheme uncertainties. We report all exposure ages assuming no erosion or snow cover (making them "apparent" exposure ages) and a sample density of 2.7g $cm^{-3}$ to maintain consistency with Johnson et al. (2020) and Adams et al., (2022). In situ $^{14}C$ AMS data and corresponding calculated exposure ages are available from the NERC UK Polar Data Centre, https://doi.org/10.5285/dbb30962-bbf3-434a-9f27-6de2f61a86e2 (Adams et al., 2024).

### 2.2 Extraction of paired $^{14}C$-$^{10}Be$ analyses from ICE-D and paired nuclide diagrams

To compare paired $^{14}C$-$^{10}Be$ exposure ages from Mt Murphy with other $^{14}C$-$^{10}Be$ datasets, we used a SQL search filter implemented in MATLAB to extract $^{14}C$-$^{10}Be$ pairs from ICE-D (Balco, 2020b), https://version2.ice-d.org/antarctica/ [last accessed 29.03.2024] which meet the following criteria: 1) the ratio of the $^{10}Be$ exposure age to the $^{14}C$ exposure age is < 4:1, and 2) the $^{10}Be$ apparent exposure age is < 11.7 ka (indicating the sample was exposed during the Holocene). We applied these filters to remove

https://doi.org/10.5194/gchron-2024-34
Preprint. Discussion started: 9 December 2024


$^{10}$Be apparent exposure ages older than the Holocene because $^{10}$Be inheritance is known to impact measurement accuracy. Sites where paired $^{10}$Be and $^{14}$C measurements satisfy the filter criteria are listed in Table 3 and numbered in Fig. 1c.

Paired nuclide diagrams (Fig. 2) represent a useful method of presenting exposure/burial histories and can potentially indicate uncertainty or help to explain scatter in a dataset (see Granger, 2006, for a detailed description of paired nuclide diagrams). We classified paired nuclide plots generated from $^{14}$C-$^{10}$Be pairs extracted from ICE-D into three distinct types: Type 1 represents a sample with simple exposure history (only one period of exposure), Type 2 represents a sample with a complex exposure history (multiple periods of exposure and burial), and Type 3 represents a sample with an impermissible concentration ratio (where an ellipse plots above the line of constant exposure in the "forbidden zone"). The Type 3 scenario can indicate analytical inconsistencies, for example, $^{14}$C contamination increasing in situ $^{14}$C concentrations (Nichols and Goehring, 2019). In certain cases, a "Type 3" nuclide ratio may be explained geologically because the constant exposure line assumes a surface production rate rather than subsurface production.

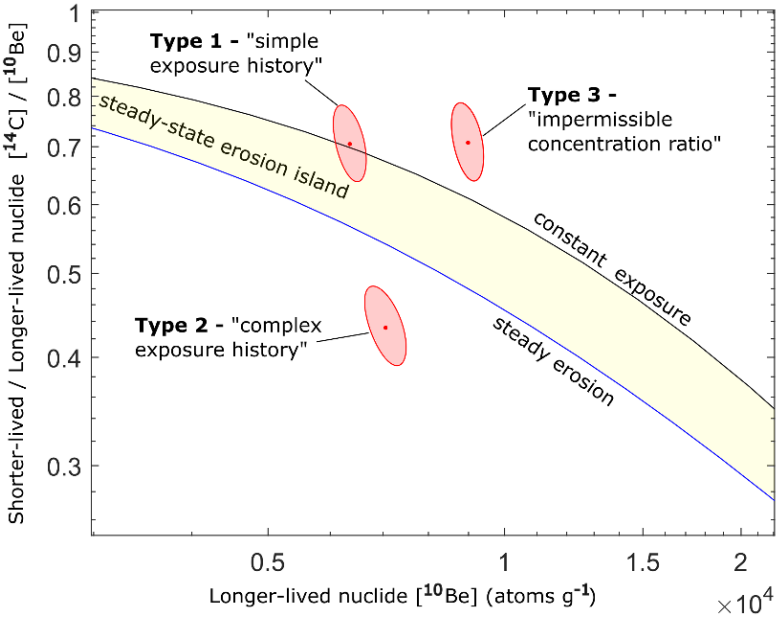


**Figure 2:** Paired nuclide diagram with key features labelled. Note that the X axis includes the concentration of the longer-lived nuclide, in this case $^{10}$Be, and the Y axis is the ratio of the concentration of the shorter- to longer-lived nuclide, in this case $^{14}$C-$^{10}$Be. Both axes are normalised to the local nuclide production rate at each sample location using the LSDn scaling model. Uncertainty ellipses (68 % confidence) are plotted using the ellipse.m code from the online calculators formerly known as the CRONUS-Earth online calculators (Balco et al., 2008). Constant exposure line (upper black), steady erosion line (lower blue), and steady-state erosion island (yellow shaded) are labelled on the figure. Paired nuclide diagram terminology from Granger (2006).

### 2.3 Investigating sources of geological uncertainty

Previous studies exhibiting concordant and discordant $^{10}$Be and $^{14}$C exposure ages (Balco et al., 2019) or seemingly impermissible $^{14}$C-$^{10}$Be concentration ratios (Rand and Goehring, 2019) have been explained by invoking geological processes. We,

https://doi.org/10.5194/gchron-2024-34
Preprint. Discussion started: 9 December 2024


therefore, investigated sources of geological uncertainty in the Mt Murphy dataset in two ways. Firstly, we compared Mt Murphy paired $^{14}C$-$^{10}Be$ exposure ages and concentrations to similar datasets identified from the filter analysis, including a discussion of the differing geological settings of Mt Murphy and other sites. Secondly, we used the search filter to identify sites with impermissible $^{14}C$-$^{10}Be$ concentration ratios (Type-3 datasets) and then, using MATLAB, modelled scenarios to reproduce the higher $^{14}C$-$^{10}Be$ concentration ratios observed in these Type-3 datasets by 1) increasing erosion rate estimates and 2) simulating a prolonged duration of burial of a sample under a thin layer of ice at shallow to moderate depths (100–2000 $g^{-1}$ $cm^2$) in the subsurface.

### 2.4 Investigating in situ $^{14}C$ reproducibility

To investigate possible sources of sample preparation uncertainty, we focus on situ $^{14}C$ reproducibility through evaluation of both new exposure age data from Mt Murphy and analysis of existing exposure age datasets in ICE-D. In situ $^{14}C$ measurement reproducibility of the new Mt Murphy analyses was assessed with the repeat measurements of four different samples. To expand the scope of the reproducibility analysis, we performed a search of the ICE-D exposure age database for all existing in situ $^{14}C$ exposure ages for which two or more measurements have been made of the same sample excluding measurements of laboratory intercomparison materials, such as CRONUS-A. After identifying samples with repeat in situ $^{14}C$ measurements from ICE-D, we determined how many repeat measurements reproduced within measurement uncertainty. To assess reproducibility, we applied a blanket measurement uncertainty of 6 % (based on the reproducibility of CRONUS-A reported from the extraction laboratory at Tulane) of the total reported in situ $^{14}C$ concentration reported from AMS measurements for each replicate. In cases where a study had reported a nuclide concentration with an associated measurement uncertainty exceeding 6 %, we used the larger value reported by the study for the reproducibility assessment.

## 3. Results

### 3.1 In situ $^{14}C$ exposure ages from Mt Murphy

Thirteen in situ $^{14}C$ measurements (including four replicate measurements) were performed on nine erratic samples recovered from Notebook Cliffs, Turtle Rock, and the un-named scoria cone from surfaces situated between 893 and 179 m a. s. l. When examining in situ $^{14}C$ reproducibility exposure ages calculated from nuclide concentrations are reported with 1 σ internal uncertainties. In situ $^{14}C$ exposure ages range from 9.0 ± 1.0 ka to 3.1 ± 0.2 ka (Table 1, Figs. 3, 4a and 4b), with an average exposure age of 6.0 ± 2.1 ka (mean and standard deviation). At scoria cone, in situ $^{14}C$ exposure ages exhibit considerable scatter over a small elevation range (180 - 240 m a. s. l.) with ages ranging from 9.0 ± 1.0 ka to 3.4 ± 0.3 ka. The spread of situ $^{14}C$ exposure ages derived from initial measured in situ $^{14}C$ concentrations is ~ 6 kyr, and some samples at higher elevations yield younger exposure ages than samples from lower elevations, which is the inverse of the expected age-elevation pattern associated with ice thinning through time. Apparent exposure ages from Notebook Cliffs (850 – 900 m a. s. l.) are 2 kyr younger than those from the scoria cone (180 – 240 m a. s. l.).

Repeat in situ $^{14}C$ measurements (n = 4) were made on samples TUR-117, TUR-132, CIN-108, and CIN-112 from the (low scoria cone 180–240 m a. s. l. and intermediate elevation (Turtle Rock, 450–650 m a. s. l.) sites. In situ $^{14}C$ exposure ages calculated

https://doi.org/10.5194/gchron-2024-34
Preprint. Discussion started: 9 December 2024


from repeat measurements range from 8.2 ± 0.8 ka to 7.2 ± 0.7 ka (Table 1, Fig. 3). Some exposure ages derived from replicate measurements reproduce within internal measurement uncertainties (at 1 σ, Fig. 3), whilst others do not. For example, in situ $^{14}$C exposure ages from TUR-117 and CIN-112 do not reproduce within range of their internal uncertainties at 1 σ (Table 1) or indeed 2 σ, with initial ages 3–5 kyr younger than those of replicate measurements. In other words, TUR-117-R, CIN-112-R are respectively 165 % and 112 % older than initial ages from the same samples, exhibiting significant scatter in excess of their internal uncertainties. CIN-108-R (7.8 ± 0.8 ka) is 24 % older than the exposure age calculated for CIN-108 (6.3 ± 0.6 ka) and does not reproduce within 1 σ internal uncertainty. TUR-132-R does, however, reproduce within 1 σ internal uncertainty. Neither the Turtle Rock nor scoria cone site show a systematic bias in terms of reproducibility, with each site yielding one unreproducible in situ $^{14}$C exposure age. There is also no correlation between sample lithology and in situ $^{14}$C reproducibility, as ages derived from both granite and gneiss samples do not reproduce within internal uncertainties. Notably, initial analyses of samples from Notebook Cliff (n = 3) and TUR-123 from > 600 m a. s. l. are systematically younger than all repeat $^{14}$C ages from samples below 500 m a. s. l. (including the reproducibility analyses, Fig. 3), which is inconsistent with the expected age-elevation pattern associated with ice thinning.

**Table 1:** New in situ $^{14}$C exposure ages from sites at Mt Murphy: Notebook Cliffs (NOT), Turtle Rock (TUR) and scoria cone (CIN). Exposure ages are reported propagating 6 % measurement uncertainties. Exposure ages were calculated using the LSDn scaling scheme. Sample IDs appended with R denote repeat measurements. See Table S1 for full in situ $^{14}$C AMS dataset.

| Sample ID | Location | Latitude DD | Longitude DD | Elevation (m a.s.l.) | Lithology | Exp. Age (ka) | Inter. Err. 1 σ (ka) | Exter. Err. 1 σ (ka) |
|---|---|---|---|---|---|---|---|---|
| TUR-123 | Turtle Rock | -75.370 | -111.292 | 639 | granite | 3.8 | 0.3 | 0.4 |
| TUR-117 | Turtle Rock | -75.381 | -111.306 | 451 | granite | 3.1 | 0.2 | 0.3 |
| TUR-132 | Turtle Rock | -75.383 | -111.309 | 446 | granite | 7.9 | 0.8 | 1.0 |
| NOT-103 | Notebook | -75.391 | -111.139 | 852 | granite | 3.8 | 0.3 | 0.4 |
| NOT-104 | Notebook | -75.388 | -111.117 | 893 | granite | 4.1 | 0.3 | 0.4 |
| NOT-107 | Notebook | -75.388 | -111.090 | 885 | granite | 5.2 | 0.4 | 0.6 |
| CIN-102 | scoria cone | -75.219 | -111.023 | 239 | gneiss | 9.0 | 1.0 | 1.3 |
| CIN-108 | scoria cone | -75.216 | -111.019 | 181 | granite | 6.3 | 0.6 | 0.7 |
| CIN-112 | scoria cone | -75.216 | -111.017 | 179 | aplite | 3.4 | 0.3 | 0.3 |
| TUR-117-R | Turtle Rock | -75.381 | -111.306 | 451 | granite | 8.2 | 0.8 | 1.1 |
| TUR-132-R | Turtle Rock | -75.383 | -111.309 | 446 | granite | 7.4 | 0.7 | 0.9 |
| CIN-108-R | scoria cone | -75.216 | -111.019 | 181 | granite | 7.8 | 0.8 | 1.0 |
| CIN-112-R | scoria cone | -75.216 | -111.017 | 179 | aplite | 7.2 | 0.7 | 0.9 |

Published $^{10}$Be exposure ages and initial in situ $^{14}$C exposure ages measured from samples TUR-132, CIN-102 and CIN-108 overlap within their respective 1 σ external uncertainties making them concordant (Fig. 4a). However, most of the paired $^{14}$C-$^{10}$Be ages (n = 6, including all NOT samples, TUR-117, TUR-123, and CIN-112) are discordant and have apparent exposure ages that are mid-late Holocene (5–3 ka). Where in situ $^{14}$C and $^{10}$Be ages are concordant, the in situ $^{14}$C age is systematically older and

https://doi.org/10.5194/gchron-2024-34
Preprint. Discussion started: 9 December 2024


early- to mid- Holocene (9–6 ka). Ages calculated from three of four replicate measurements overlap at 1 σ external uncertainty with the corresponding $^{10}$Be exposure ages (Fig. 4b). However, the in situ $^{14}$C exposure age calculated from the repeat measurement of sample CIN-108 is discordant with the $^{10}$Be exposure age from the same sample. We note the initial in situ $^{14}$C measurement of CIN-108 resulted in a concordant $^{14}$C-$^{10}$Be exposure age pair.

We now compare paired nuclide diagrams of $^{14}$C-$^{10}$Be concentration data from Mt Murphy. Based on initial in situ $^{14}$C concentrations, samples from Notebook Cliffs, Turtle Rock, and scoria cone (Fig. 5a) can be classified as Type 1, Type-2 and to an extent Type-3 nuclide ratios (see section 2.3). Samples TUR-132, CIN-102 and CIN-108 plot within the steady-state erosion island (Type-1) and display concordant in situ $^{14}$C and $^{10}$Be exposure ages (Fig. 5a). The remaining samples (NOT-103, NOT-104, TUR-123, TUR-117, and CIN-112) yield paired $^{14}$C and $^{10}$Be nuclide concentrations that plot below the steady state erosion line and thus indicate complex exposure histories (Type-2). Samples plotting below the steady erosion line (n = 6) include all the young in situ $^{14}$C ages which are discordant with respect to the $^{10}$Be exposure age from the same sample. TUR-138, for which both $^{10}$Be and in situ $^{14}$C were measured for an earlier study of Mt Murphy (Johnson et al., 2020), displays an impermissible $^{14}$C-$^{10}$Be ratio (Type-3).

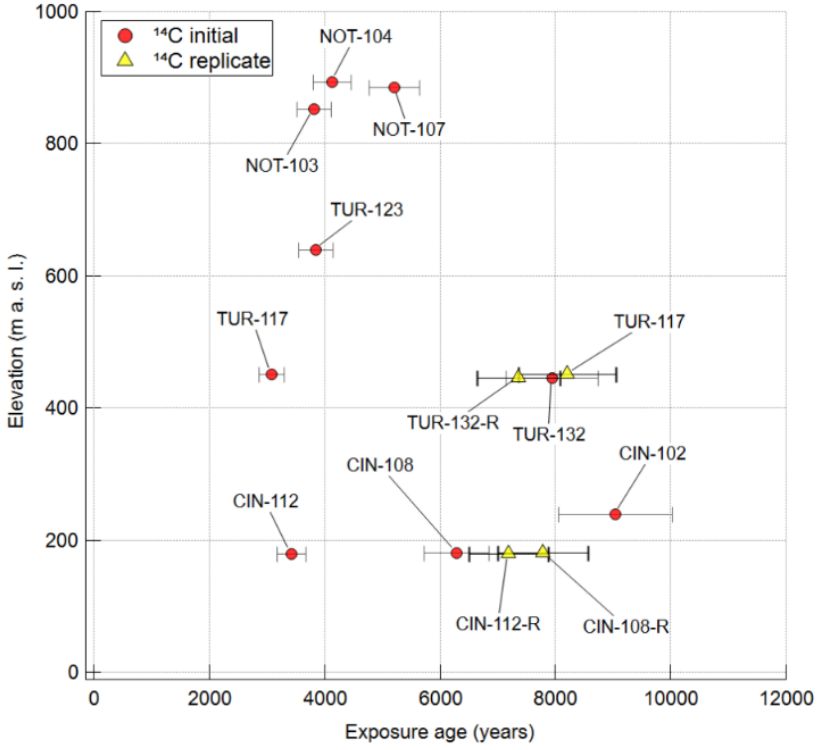


**Figure 3**: Plot of in situ $^{14}$C ages vs elevation comparing in situ $^{14}$C exposure ages calculated from both initial and replicate in situ $^{14}$C concentrations. Ages derived from initial in situ $^{14}$C concentrations are depicted by red circles and ages derived from replicate concentrations by yellow triangles. In situ $^{14}$C exposure ages are plotted with 1 σ internal uncertainties calculated from the 6 % measurement uncertainty applied to in situ $^{14}$C concentrations**.** Replicate in situ $^{14}$C uncertainty bars displayed with thicker lines.

https://doi.org/10.5194/gchron-2024-34
Preprint. Discussion started: 9 December 2024


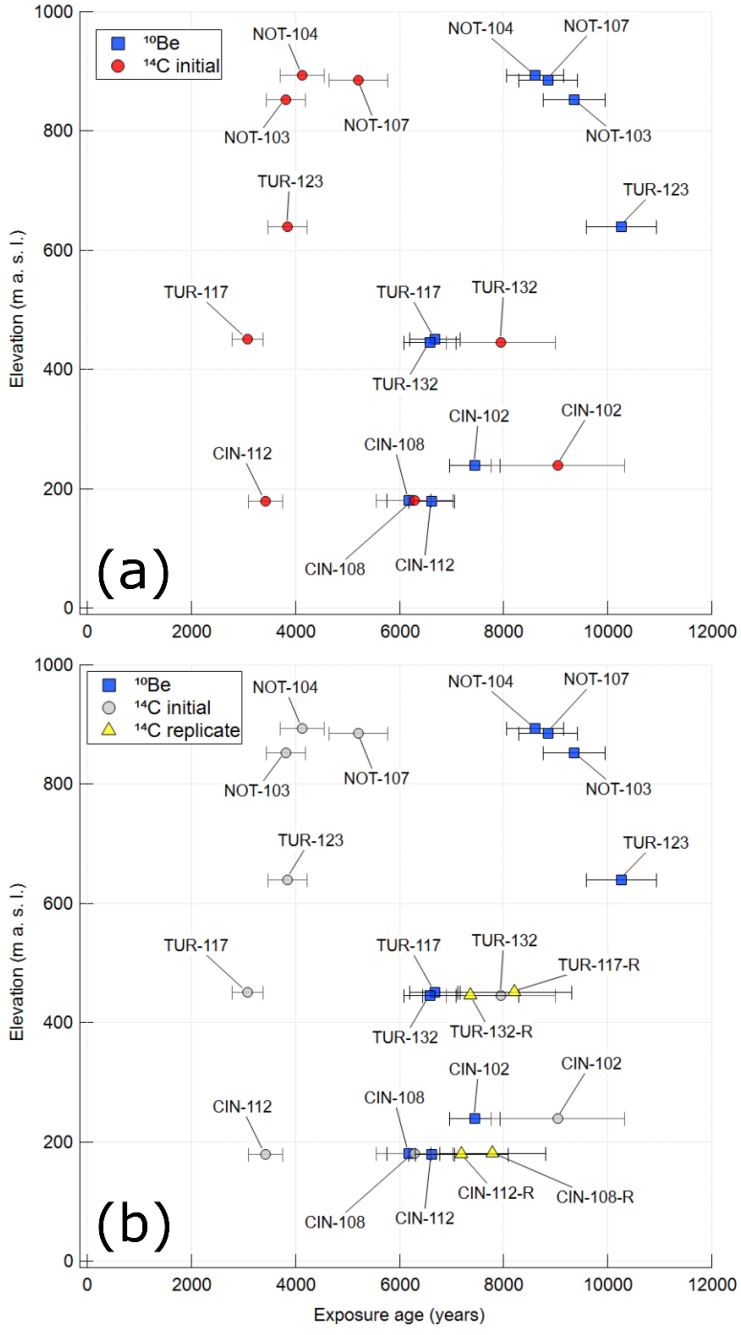


**Figure 4:** Mt Murphy paired $^{14}$C-$^{10}$Be exposure age versus elevation plots **(a)** calculated using initial in situ $^{14}$C concentrations and **(b)** using both initial (greyed-out) and replicate in situ $^{14}$C concentrations. In situ $^{14}$C exposure ages plotted with 1σ external uncertainties following propagation of nominal 6 % in situ $^{14}$C measurement uncertainties. We report exposure ages with 1 σ external uncertainties when comparing exposure ages calculated from in situ $^{14}$C and $^{10}$Be concentrations measured in the same sample (see Methods section 2.1).

https://doi.org/10.5194/gchron-2024-34
Preprint. Discussion started: 9 December 2024


When comparing the replicate in situ $^{14}C$ measurements three paired $^{14}C$-$^{10}Be$ concentration ratios plot within the steady state erosion island (Fig. 5b), indicating these samples experienced a simple exposure history (Type 1). The position of sample TUR-132-R is comparable to its position when plotted using the initial measured in situ $^{14}C$ concentration. In contrast, using initial $^{14}C$ concentrations, TUR-117 and CIN-112 plot below the steady erosion line, suggesting complex exposure histories (Type-2). The positions of TUR-117 and CIN-112 on the paired isotope plot (Type-2) are consistent with in situ $^{14}C$ exposure ages that exhibit discordance with $^{10}Be$ ages from the same sample (Fig. 4a). Older in situ $^{14}C$ exposure ages calculated from repeat measurements (TUR-117-R, CIN-112-R; Fig. 4b) are, however, consistent with Type-1 $^{14}C$-$^{10}Be$ concentration ratios (suggestive of simple exposure histories).

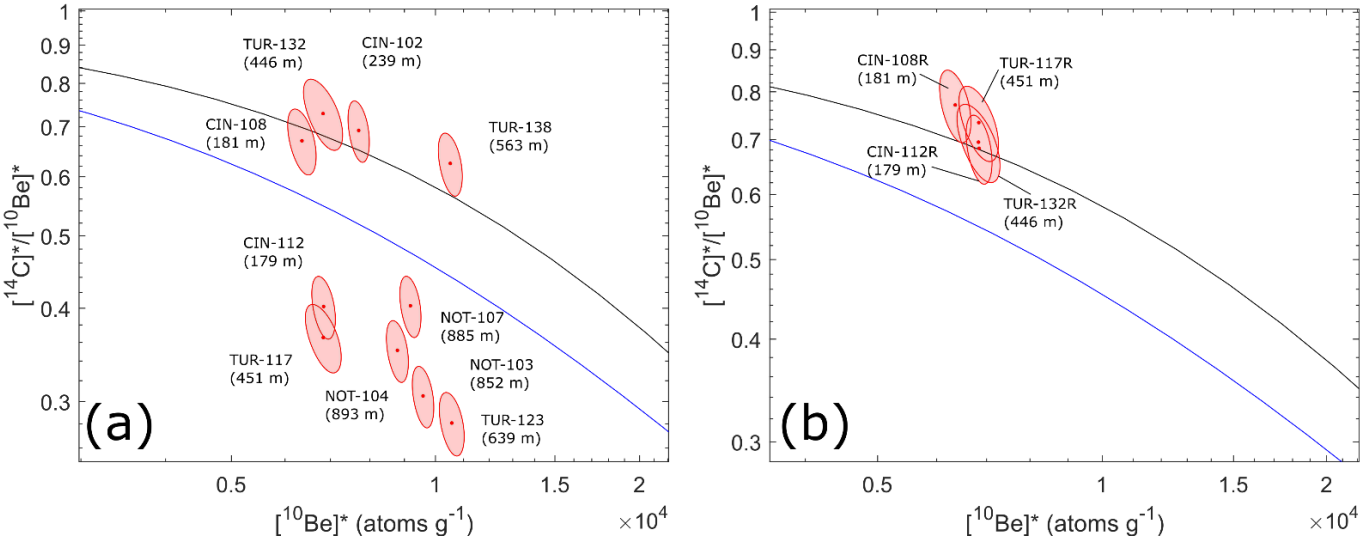


**Figure 5:** Paired $^{14}C$-$^{10}Be$ nuclide diagrams using new in situ $^{14}C$ concentrations from Mt Murphy samples. Panel **(a)** shows $^{14}C$-$^{10}Be$ nuclide ratios using initial in situ $^{14}C$ concentrations and panel **(b)** shows $^{14}C$-$^{10}Be$ ratios using in situ $^{14}C$ concentrations from repeat measurements. The *x*-axis represents the $^{10}Be$ concentration normalised to its production rate (atoms $g^{-1}$ $yr^{-1}$) and the *y*-axis represents the ratio of the concentration of $^{14}C$, the shorter half-life nuclide, normalised by its production rate to $^{10}Be$ – the longer-lived nuclide. Ellipses are plotted using the LSDn scaling scheme (68 % confidence). In situ $^{14}C$ extraction for TUR-138 (panel **a**) was performed at LDEO.

### 3.2 Analysis of paired $^{14}C$-$^{10}Be$ measurements in ICE-D.

Following examination of $^{10}Be$ and in situ $^{14}C$ exposure ages from Mt Murphy we now investigate other locations with paired $^{14}C$-$^{10}Be$ measurements. Specifically, we look at sites within (Fig. 1b) and outside (Fig. 1c) Antarctica in which i) the ratio of the $^{10}Be$ exposure age to the $^{14}C$ exposure age is < 4:1, and ii) the $^{10}Be$ exposure age is Holocene (< 11.7 ka). A summary of all sites with paired $^{14}C$-$^{10}Be$ exposure ages returned from ICE-D that satisfy our search criteria (n = 29, Fig. 1) is provided in Table 2, and age vs elevation plots and paired nuclide diagrams can be viewed in Supplement S4. The total number of paired in situ $^{14}C$-$^{10}Be$ measurements of Holocene age (n = 255) at the time of extraction from ICE-D [last accessed - 29.03.2024] is low compared to the over 28,000 total paired $^{26}Al$-$^{10}Be$ measurements in ICE-D (although many predate the Holocene). We identify three endmember

https://doi.org/10.5194/gchron-2024-34
Preprint. Discussion started: 9 December 2024


datasets with paired nuclide diagrams that exhibit a predominant Type 1, 2, or 3 $^{14}C$-$^{10}Be$ concentration ratio (Fig. 6). We observe Type-1 paired $^{14}C$-$^{10}Be$ concentrations (indicative of simple exposure) at Kangiata Nunata Sermia (KNS), Greenland (Young et al., 2021; Fig. 6b). Type-2 $^{14}C$-$^{10}Be$ concentrations (indicative of complex exposure) are observed in the forefield of the Rhône Glacier (Goehring et al., 2011). Finally, Type-3 $^{14}C$-$^{10}Be$ concentrations (indicative of "forbidden" exposure histories) are observed on the Antarctic Peninsula, proximal to the Sjögren Glacier (Balco and Schaefer, 2013). The Mt Murphy $^{14}C$-$^{10}Be$ dataset displays elements of all three types, including those observed at KNS (Type-1), Rhône Glacier, Switzerland (Type-2) and to a limited extent Sjögren Glacier. Type-1 exposure ages from this present study (e.g., CIN-108, TUR-132, CIN-102) are most similar to paired $^{14}C$-$^{10}Be$ measurements from KNS, Greenland (Young et al., 2021, Fig. 6b). Type-2 concentrations in this present study (e.g. NOT-103, NOT-104, CIN-112, TUR-117) are comparable to paired $^{14}C$-$^{10}Be$ concentrations from the Rhône Glacier, Switzerland (Goehring et al., 2011, Fig. 6c). Finally, $^{14}C$-$^{10}Be$ concentration ratios observed at Sjögren Glacier (Balco and Schaefer, 2013, Fig. 6d) mostly plot above the simple exposure line (Type-3). In addition, some paired $^{14}C$-$^{10}Be$ concentrations from Conness Glacier forefield in the Sierra Nevada Range, California (Jones et al., 2023) plot as non-uniform ellipses. These are all, however, associated with very young exposure ages (last few hundred years), and so are not discussed further here. Focusing on the conditions surrounding each of the three endmember $^{14}C$-$^{10}Be$ datasets may help explain our observations from the Mt Murphy paired $^{14}C$-$^{10}Be$ dataset.

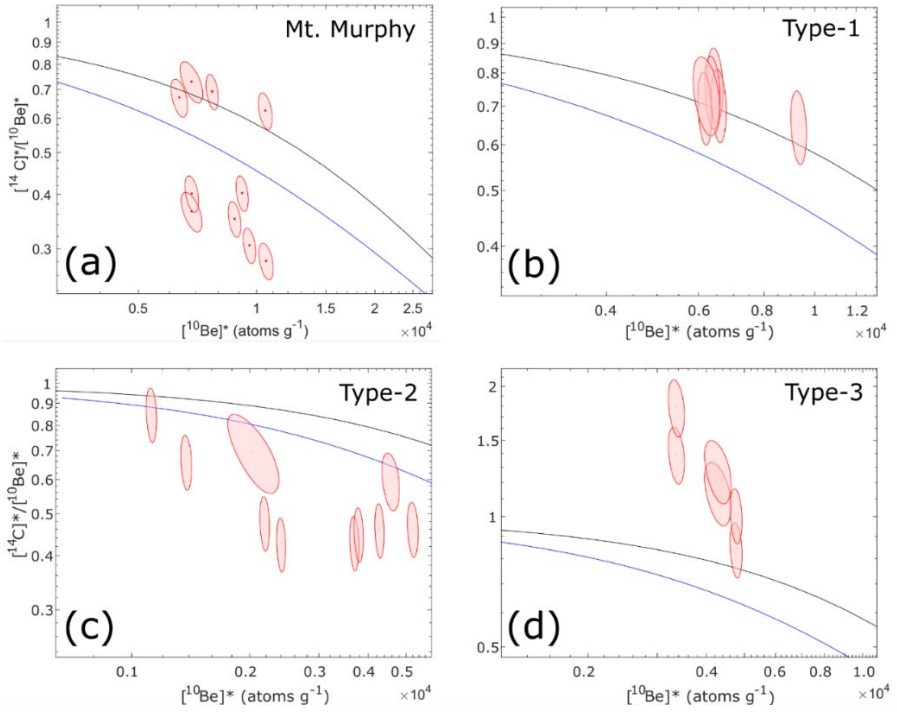


**Figure 6:** Paired in situ $^{14}C$-$^{10}Be$ nuclide concentrations from **(a)** Mount Murphy, **(b)** Kangiata Nunata Sermia (KNS), Greenland (Type-1, dominated by concordant ages), **(c)** Rhône Glacier, Switzerland, (Type 2, complex exposure – burial history) and **(d)** Sjögren Glacier, Antarctic Peninsula (Type 3 – "impermissible" exposure history-dominated dataset). NB: Other paired $^{14}C$-$^{10}Be$ datasets classified using the same system are displayed in Table 2. All paired $^{14}C$-$^{10}Be$ concentration ratios are normalised to the sample-specific production rate using the LSDn scaling scheme (Lifton et al., 2014). For further information on paired nuclide diagrams and "Type" classification scheme, see section 2.3.

https://doi.org/10.5194/gchron-2024-34
Preprint. Discussion started: 9 December 2024


### 3.3 Geological uncertainty and modelled subsurface production scenarios

#### 3.3.1 Tucker Glacier and Mt Murphy age vs elevation datasets

Our first assessment of geological uncertainty compares paired $^{14}C$-$^{10}Be$ ages from Mt Murphy and Tucker Glacier in the Ross Sea Embayment of Antarctica. Tucker Glacier does not meet the second search criteria ($^{10}Be$ ages < 11.7 ka) but shares many characteristics with the Mt Murphy dataset. These characteristics include many samples with paired $^{14}C$-$^{10}Be$ measurements, a relatively large degree of scatter in nuclide concentrations from samples at the same elevations, and a mixture of concordant and discordant paired in situ $^{14}C$-$^{10}Be$ exposure ages (Fig. 7a). The youngest in situ $^{14}C$ ages at this site are also discordant with respect to corresponding $^{10}Be$ ages. The distribution of exposure ages from Shark Fin is similar to the Mt Murphy dataset (Fig. 4) when plotted with elevation. Paired $^{14}C$-$^{10}Be$ concentration ratios are, however, largely consistent with simple exposure histories (Fig. 7b).

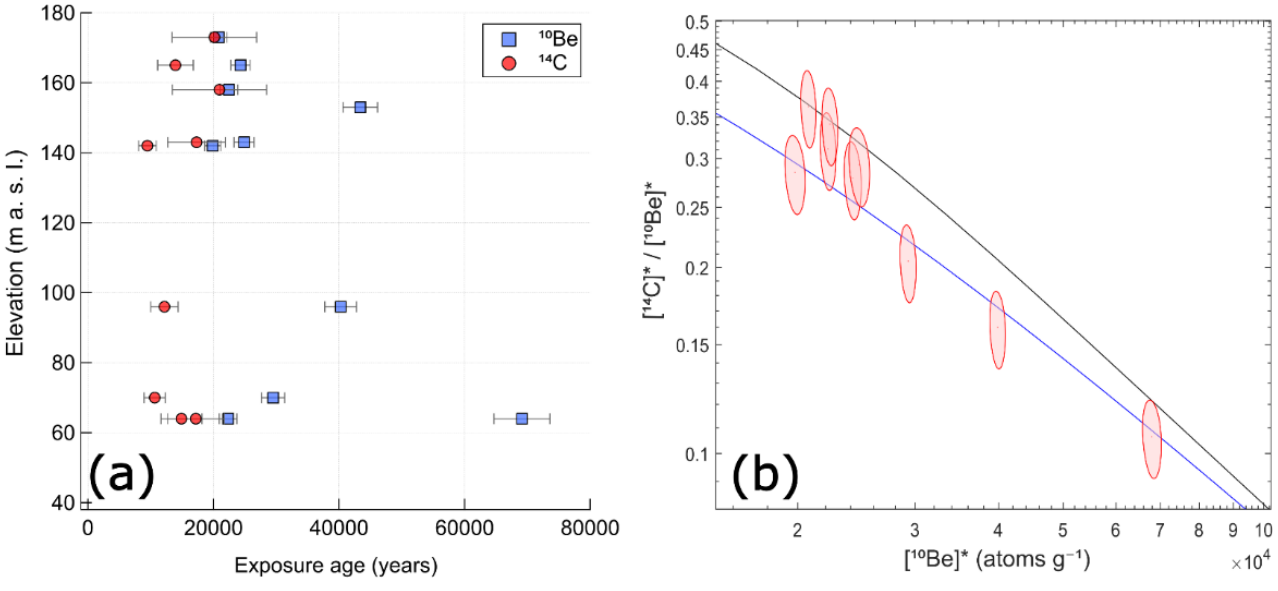


**Figure 7:** Paired $^{14}C$-$^{10}Be$ exposure ages **(a)** and paired nuclide diagram **(b)** from Shark Fin nunatak, Antarctica. Error bars in panel **a** represent 1σ external uncertainties as in situ $^{14}C$ and $^{10}Be$ production rates in the study were derived from different calibration datasets, one in situ $^{14}C$ sample was saturated so is not displayed. In situ $^{14}C$ exposure age uncertainties are plotted following propagation of a nominal 6 % internal uncertainty following the original study of Balco et al. (2019).

#### 3.3.2 Increased $^{14}C$-$^{10}Be$ ratio by higher in situ $^{14}C$ subsurface production by muons relative to $^{10}Be$

Our second assessment of geologic uncertainty models scenarios where samples are subject to either rapid exhumation from ice, or prolonged burial under ice, leading to higher in situ $^{14}C$ production relative to $^{10}Be$ production in the subsurface (see section 1.1).

https://doi.org/10.5194/gchron-2024-34
Preprint. Discussion started: 9 December 2024


In both scenarios the in situ $^{14}C$ nuclide concentration is expected to increase relative to $^{10}Be$ and may explain impermissible Type-3 $^{14}C$-$^{10}Be$ concentration ratios observed at Sjögren Glacier (see Sect. 2.4).

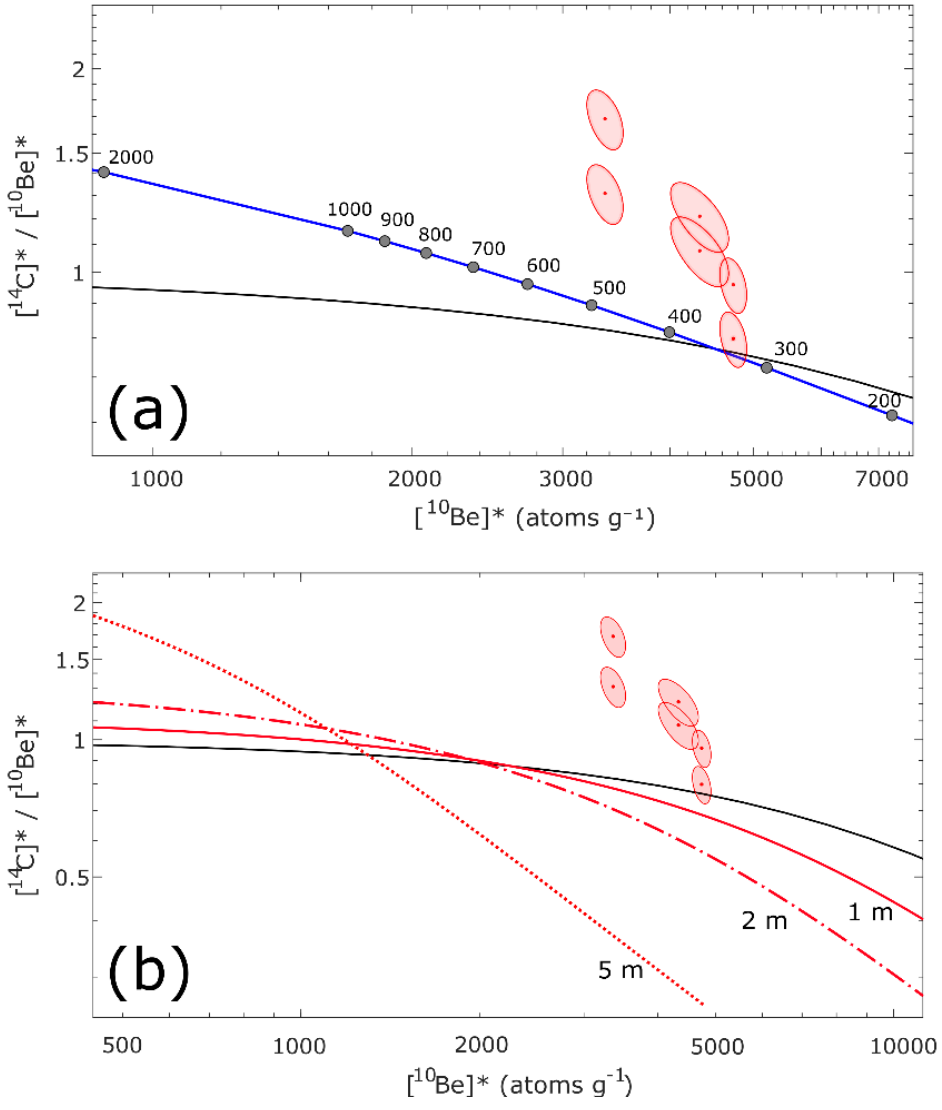


**Figure 8:** Plots showing modelled subsurface production scenarios that lead to a higher in situ $^{14}C$ relative to $^{10}Be$ ratio than typical for the surface. Panel (**a**) shows $^{14}C$ -$^{10}Be$ nuclide ratios as a function of erosion rate integrated over a time t, assuming both $^{10}Be$ and in situ $^{14}C$ nuclide concentrations are zero at the LGM (t = 20000 years). The black line represents the constant exposure line and blue line the steady erosion line including muon production. Grey dots indicate modelled $^{14}C$-$^{10}Be$ nuclide concentration ratios for an erosion rate which is specified above each dot (mm kyr$^{-1}$). Panel (**b**) shows modelled $^{14}C$-$^{10}Be$ nuclide concentrations as a function of burial under different ice thicknesses over Holocene timescales (plotted as isolines). The black line represents the constant exposure line, but we omit the steady erosion line to improve legibility. On both plots red ellipses indicate $^{14}C$-$^{10}Be$ concentration ratios measured in samples from Sjögren Glacier, Site C (68 % confidence). Plots are generated using the surface and subsurface production rate estimating code from Balco et al., (2023).

https://doi.org/10.5194/gchron-2024-34
Preprint. Discussion started: 9 December 2024


We first model rapid exhumation of a sample from overlying ice, which can be thought of as increasing the erosion rate, to investigate if this scenario would yield $^{14}C$-$^{10}Be$ ratios comparable to ratios observed in Sjogren Glacier samples (Fig. 8a). We observe that an increase in erosion rate to between 1000–2000 mm kyr$^{-1}$ results in high modelled $^{14}C$-$^{10}Be$ ratios (> 1.5), comparable to ratios observed in the Sjögren Glacier samples. Faster erosion rates, however, also result in modelled $^{10}Be$ concentrations of < 2000 atoms g$^{-1}$, considerably lower than $^{10}Be$ concentrations measured in the Sjögren Glacier samples. At slower erosion rates of 300–400 mm kyr$^{-1}$, the modelled $^{10}Be$ concentration is comparable to concentrations at Sjögren Glacier, but the modelled $^{14}C$-$^{10}Be$ ratio is < 1, which is much lower than the high $^{14}C$-$^{10}Be$ ratio of most Sjögren Glacier samples.

We model for a second scenario whereby a sample is buried at specific depths of 1, 2 and 5 metres under ice, over Holocene timescales (Fig. 8b). For this scenario, we observe that significant burial at depths below 2–3 metres are required generate a high modelled $^{14}C$-$^{10}Be$ ratio which is comparable with ratios observed in Sjogren Glacier samples. Burial under 5 metres of ice increases the $^{14}C$-$^{10}Be$ ratios to match the highest ratios observed at Sjögren Glacier. However, the $^{10}Be$ nuclide concentration is extremely low at these ratios (< 1000 at g$^{-1}$).

### 3.4 Sample preparation uncertainty - Mt Murphy and ICE-D in situ $^{14}C$ reproducibility

We now describe results of new in situ $^{14}C$ repeat measurements from Mt Murphy and repeat measurements extracted from ICE-D (Fig. 9). Although the Mt Murphy sample size is small (n = 4) it is notable that 3 out of 4 in situ $^{14}C$ concentrations do not replicate within the 1σ 6 % measurement uncertainty (Fig. 4), and 2 of 4 in situ $^{14}C$ concentrations do not replicate at 2 σ. In addition to the Mt Murphy results, a further 25 samples for with repeat in situ $^{14}C$ measurements are also in ICE-D, and a further two samples with replicate in situ $^{14}C$ measurements from the Leymon High Core (Lupker et al., 2015) bringing the total number of samples for which multiple in situ $^{14}C$ measurements exist to 31. The majority of replicates are from samples sourced from the Antarctic Peninsula (n = 5; Balco and Schaefer, 2013), Weddell Sea Embayment (n = 5; Nichols et al., 2019), Promontory Point (Pleistocene Lake Bonneville), Utah (n = 5; Lifton et al., 2015a) and the Northwest Highlands, Scotland (n = 5; Borchers et al., 2016). From these 31 samples with replicate in situ $^{14}C$ measurements, we observe 18 of the 31 samples display one or more in situ $^{14}C$ measurements that do not replicate within a 6 % 1σ measurement uncertainty (Fig. 9). There is a slight improvement in reproducibility at 2 σ, however, 15 of 31 samples still exhibit one or more in situ $^{14}C$ measurements that are not reproducible (see Fig. S9).

https://doi.org/10.5194/gchron-2024-34
Preprint. Discussion started: 9 December 2024


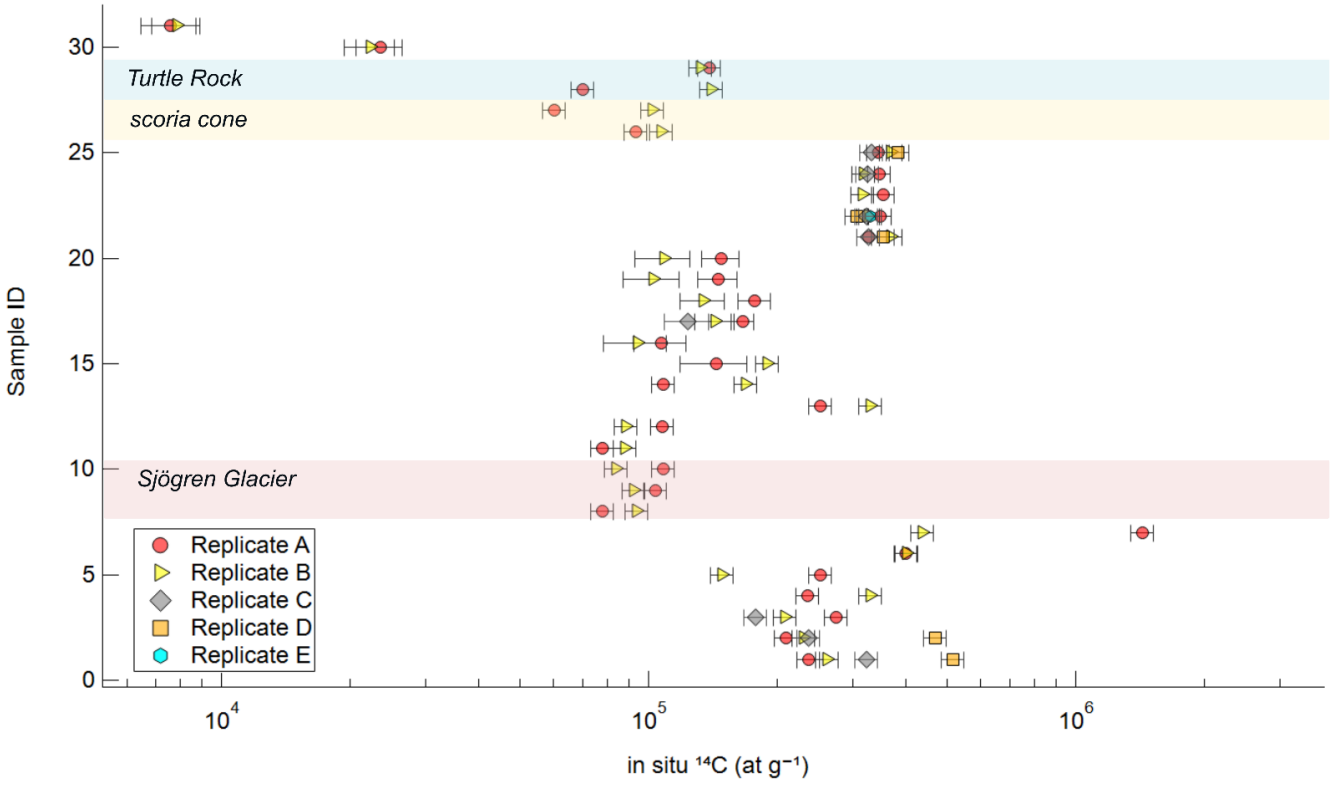


**Figure 9:** In situ $^{14}C$ concentrations in ICE-D with one or more replicate measurements from the same sample (n = 31). To enable comparison with the Mt Murphy dataset, in situ $^{14}C$ concentration error bars represent a 6 % measurement uncertainty based on repeatability of CRONUS-A measured at Tulane (Goehring et al., 2019a). The graph displays all samples with repeat in situ $^{14}C$ concentrations uploaded to ICE-D as of 29th March 2024 as well as repeat in situ $^{14}C$ measurements from Mt Murphy samples (this study) and Leymon High bedrock core samples (Lupker et al., 2015). We did not include in situ $^{14}C$ concentrations reported from Interlaboratory comparison materials such as CRONUS-A. We use the measurement uncertainty reported with a particular study when this value exceeds the nominal 6 % 1σ uncertainty. Replicate in situ $^{14}C$ measurements discussed in the text; Turtle Rock, scoria cone and Sjögren Glacier are indicated by shading. See Table S3 for full list of Sample ID's and corresponding sites.

**Table 2 (Overleaf)**: Full list of paired $^{14}C$-$^{10}Be$ surface exposure ages extracted from ICE-D using the following filters: i) apparent $^{10}Be$ exposure age is < 4x than apparent $^{14}C$ exposure age ii) $^{10}Be$ exposure ages are of Holocene age (< 11.7 ka). Paired nuclide ratio type refers to the dominant position of paired $^{14}C$-$^{10}Be$ ratio ellipses on the paired nuclide diagram. Paired nuclide diagrams from each site feature one Type, e.g., 1, 2 or 3 or a mixture of types. Instances of the secondary less dominant type are denoted in brackets. Abbreviations for AMS and in situ $^{14}C$ extraction laboratories are as follows; CEREGE (Centre Européen de Recherche et d'Enseignement des Géosciences de l'Environnement), ETH Zurich (Swiss Federal institute of Technology in Zurich), (KIST (Korean Institute of Science and Technology), LDEO (Lamont Doherty Earth Observatory), LLNL (Lawrence Livermore National Laboratory), NOSAMS (National Ocean Sciences Accelerator Mass Spectrometer Laboratory at the Woods Hole Oceanographic Institute) and SUERC (Scottish Universities Environmental Research Centre). Shark Fin nunatak $^{10}Be$ ages are > 11.7 ka, so do not meet one of our search criteria but are included here due to the similarities in the age vs elevation profile of Shark Fin nunatak and the Mt Murphy data. #Engabreen glacier paired $^{14}C$-$^{10}Be$ data are not in ICE-D but are included to demonstrate a geological solution to a paired $^{14}C$-$^{10}Be$ "Type 3" dataset. *Unpublished in situ $^{14}C$ data obtained from the informal cosmogenic-nuclide exposure age database (ICE-D). These data are, however, freely available in ICE-D under the public release requirements of the National Science Foundation (NSF) U.S. Antarctic Program which requires data be made publicly available 2 years after collection.

| Location ID | Short Name (ICE-D) | Site Name, Location | $^{14}C$-$^{10}Be$ ratio | In situ $^{14}C$ extraction | AMS lab $^{14}C$ | Reference $^{10}Be$ dataset | Reference in situ $^{14}C$ dataset |
|---|---|---|---|---|---|---|---|
| 1 | REA | Mt.Rea, Sarnoff Mts. | 3 | Tulane | NOSAMS | Stone et al., (2003) | ICE-D* |
| 2 | TR | Turtle Rock, Mt Murphy | 1 2 (3) | Tulane | NOSAMS | Johnson et al., (2020) | This paper(Johnson et al., 2020) |
| 3 | NMAS | North Masson Range, Framnes Mts. | 3 (1) | SUERC | SUERC | Mackintosh et al., (2007) | White et al., (2011) |
| 4 | SKF | Sharkfin nunatak, Tucker Gl. | 1 (2) | Tulane | LLNL | Balco et al., (2019) | Balco et al., (2019) |
| 5 | MZS | Mario Zuchelli Station, Terra Nova Bay | 1 | Tulane | LLNL | Goehring et al., (2019b) | Goehring et al., (2019b) |
| 6 | WHITS | Mt. Whitmore, Whitmore Mts. | N/A | Tulane | NOSAMS | Spector et al., (2019) | Spector et al., (2019) |
| 7 | KAYCONE | scoria cone, Mt Murphy | 1 2 | Tulane | NOSAMS | Adams et al., (2022) | This paper |
| 8 | NOTE | Notebook Cliffs, Mt Murphy | 2 | Tulane | NOSAMS | Johnson et al., (2020) | This paper |
| 9 | HOPE | Mt. Hope, Beardmore Glacier | 2 (1) | Tulane | NOSAMS | Spector et al., (2017) | ICE-D* |
| 10 | CMARSH | Cape Marsh, Robertson Island | 1 | KIST | KIST | Jeong et al., (2018) | Jeong et al., (2018) |
| 11 | FRAMNES | Cape Framnes, Jason Peninsula | 1 (2) | KIST | KIST | Jeong et al., (2018) | Jeong et al., (2018) |
| 12 | SJOC | Site C, Sjogren-Boydell Fjord | 3 | Tulane | NOSAMS | Balco and Schaefer, (2013) | ICE-D* |
| 13 | DRYE | Site E, Drygalski Glacier | 1 (2) | Tulane | NOSAMS | Balco and Schaefer, (2013) | ICE-D* |
| 14 | KRING | Mt. Kring, David Glacier | 3 | Tulane | NOSAMS | Stutz et al., (2021) | ICE-D* |
| 15 | DIAMOND | Diamond Hill, Darwin-Hatherton Glaciers | 3 | Tulane | NOSAMS | Hillebrand et al., (2021) | Hillebrand et al., (2021) |
| 16 | DANPB1 | Danum Platform, Darwin-Hatherton Glaciers | 1 (3) | Tulane | NOSAMS | Hillebrand et al., (2021) | Hillebrand et al., (2021) |
| 17 | Goeh2011-A | Rhône Glacier, Swiss Alps | 2 | LDEO | Uni of Arizona | Goehring et al., (2011) | Goehring et al., (2011) |
| 18 | Hipp2014-A | Gotthard Pass, Swiss Alps | 1 | ETH Zurich | ETH Zurich | Hippe et al., (2014) | Hippe et al., (2014) |
| 19 | KBR1 | KNS bedrock 1, Kangiata Nunata Sermia | 1 | LDEO | CEREGE | Young et al., (2021) | Young et al., (2021) |
| 20 | KBR2 | KNS bedrock 2, Kangiata Nunata Sermia | 1 | LDEO | CEREGE | Young et al., (2021) | Young et al., (2021) |
| 21 | INGLE1 | Outboard ice margin, Inglefield Land | 1 | ETH Zurich | ETH Zurich | Søndergaard et al., (2020) | Søndergaard et al., (2020) |
| 22 | MACAULAY | Macaulay Boulder Field, Southern Alps | 1 (3) | LDEO | LLNL-CAMS | Putnam et al., (2010) | (Schimmelpfennig et al., 2012) |
| 23 | MARRAIT | Marrait Moraine, Jakobshavn Isfjord | 1 | LDEO | LLNL-CAMS | Young et al., (2013) | Young et al., (2014) |
| 24 | GHm-Out5 | Grey Hunter massif, MacArthur Mts., Yukon | 1 | Tulane | NOSAMS | Goehring et al., (2022) | Goehring et al., (2022) |
| 25 | SISPEN-W | Sisimiut Peninsula, Kangerlassuaq | 1 | LDEO | CEREGE | Sbarra et al., (2022) | Sbarra et al., (2022) |
| 26 | Mammoth-Forefield | Mammoth Gl., Wind River Range, WY | 1 | Tulane | NOSAMS | Jones et al., (2023) | Jones et al., (2023) |
| 27 | Conness-Forefield | Conness Gl., Sierra Nevada, CA | 1 2 3 | Tulane | NOSAMS | Jones et al., (2023) | Jones et al., (2023) |
| 28 | JIF-Forefield | Juneau Ice Field, Coast Mts., AK | 1 2 3 | Tulane | NOSAMS | Jones et al., (2023) | Jones et al., (2023) |
| 29 | N/A | Engabreen Glacier, Norway[#] | 3 | Tulane | NOSAMS | Rand and Goehring, (2019) | Rand and Goehring, (2019) |



https://doi.org/10.5194/gchron-2024-34
Preprint. Discussion started: 9 December 2024


GEOCHRONOLOGY Discussions
Open Access
EGU

https://doi.org/10.5194/gchron-2024-34
Preprint. Discussion started: 9 December 2024


## 4. Discussion

This study compares new in situ $^{14}C$ exposure ages from Mt Murphy with published $^{10}Be$ ages from the same samples. A total of 3 of 4 new in situ $^{14}C$ repeat measurements do not replicate within their 1σ internal uncertainties (Fig. 4), and samples with concordant and discordant $^{14}C$-$^{10}Be$ exposure ages suggest both simple and complex exposure histories at the same elevation (Fig. 4 and Fig. 5). Results from the filter analysis of Holocene $^{14}C$-$^{10}Be$ exposure ages in ICE-D (Table 2) indicate some $^{14}C$ and $^{10}Be$ nuclide pairs exhibit Type-3 (impermissible) $^{14}C$-$^{10}Be$ ratios (Fig. 6). We also identify a total of 31 samples from Mt Murphy, ICE-D [last accessed - 29.03.2024] and literature sources for which multiple in situ $^{14}C$ measurements have been made. Of these, 18 samples exhibit at least one repeat in situ $^{14}C$ measurement that does not reproduce within a 6 % 1σ internal measurement uncertainty (Fig. 9).

### 4.1 Key observations from the Mt Murphy paired $^{14}C$-$^{10}Be$ exposure ages

We begin the discussion focusing on key results from the Mt Murphy paired $^{14}C$-$^{10}Be$ exposure ages, and corresponding $^{14}C$-$^{10}Be$ ratios. Three of the four replicate in situ $^{14}C$ measurements, yield exposure ages that do not overlap within internal uncertainty (1σ) with initial $^{14}C$ exposure ages from the same sample (Fig. 3). TUR-117-R and CIN-112-R also do not replicate at 2 σ internal uncertainty with initial $^{14}C$ exposure ages from the same sample. These initial in situ $^{14}C$ exposure ages suggest deglaciation from 5–3 ka and are discordant with $^{10}Be$ exposure ages from TUR-117 and CIN-112. TUR-117 and CIN-112 yielded two of the six exposure ages calculated from initial in situ $^{14}C$ measurements of samples ranging from 150–900 m a. s. l. which were systematically young (5–3 ka, Fig. 4a). These systematically young in situ $^{14}C$ exposure ages appear to contradict the currently interpreted deglacial history that the ice surface at Mt Murphy lowered to an elevation of ~ 150 m a. s. l. by 6 ka (Johnson et al., 2020; Adams et al., 2022; Balco et al., 2023). In addition, the young discordant in situ $^{14}C$ exposure ages from higher elevations (Notebook Cliffs and TUR-123) and older reproducible in situ $^{14}C$ ages from lower elevations are inverted with respect to and contradict the expected age-elevation pattern associated with ice thinning. The two samples measured for in situ $^{14}C$ that did reproduce within their uncertainties at 2 σ (TUR-132 and CIN-108) were also concordant in respect to existing $^{10}Be$ exposure ages from the same sample (Fig. 4b). From the Mt Murphy replicate measurements (n = 4), the two young in situ $^{14}C$ ages are not reproducible at 2 σ internal uncertainty, but both older exposure ages are reproducible at 2 σ internal uncertainty. In summary, Mt Murphy paired $^{14}C$-$^{10}Be$ exposure ages display both concordance and discordance across multiple sites. Concordant exposure ages are consistent with Type-1 $^{14}C$-$^{10}Be$ ratios and discordant exposure ages consistent with Type-2 (and Type-3) $^{14}C$-$^{10}Be$ ratios. Concordant $^{14}C$-$^{10}Be$ exposure ages exhibit in situ $^{14}C$ ages which are reproducible at 2 σ internal uncertainty whereas discordant $^{14}C$-$^{10}Be$ exposure ages do not.

A bootstrap linear regression analysis (see Supplement 2) of in situ $^{14}C$ and $^{10}Be$ exposure age datasets from Kay Peak and a scoria cone adjacent to Kay Peak indicate in situ $^{14}C$ and $^{10}Be$ chronologies are broadly similar with respect to the timing of deglaciation, implying they are equally accurate (see Fig. S10). There is, however, significant excess scatter of ~1849 years in the in situ $^{14}C$ ages (Supplement S2, Table S4) that cannot be accounted for by the nominal 6 % 1σ internal measurement uncertainty

https://doi.org/10.5194/gchron-2024-34
Preprint. Discussion started: 9 December 2024


for in situ $^{14}$C adopted in many studies (e.g., Balco et al., 2019; Nichols et al., 2019). The new in situ $^{14}$C exposure ages and existing $^{10}$Be exposure data and $^{10}$Be-$^{14}$C ratios from Mt Murphy (Fig. 4, Fig. 5) raise two important questions: 1) Is there a geological explanation for co-existence of concordant and discordant paired in situ $^{14}$C and $^{10}$Be exposure ages, often at the same elevation, as well as a mix of Type 1, Type 2 (and Type-3) $^{14}$C-$^{10}$Be ratios? and 2) Is there a way to explain why 3 of 4 replicate in situ $^{14}$C analyses which do not produce within their 6 % 1σ internal measurement uncertainties? The second question is especially pertinent because there cannot be a geological explanation for large variations in concentrations of the same nuclide from the same sample.

### 4.2 A Geological explanation for paired $^{14}$C-$^{10}$Be sample concordance and discordance

First, we examine the Notebook Cliffs, Turtle Rock, and scoria cone sites to determine if localised geological changes at Mt Murphy permit the existence of paired $^{14}$C-$^{10}$Be discordant exposure ages at the same elevation as paired $^{14}$C-$^{10}$Be concordant exposure ages. A trimetrogon aerial flightline photo shows that in 1966, in contrast to today, the lower scoria cone outcrop was almost completely buried by ice. This finding indicates that samples CIN-112 and CIN-108 were shielded by ice for a non-zero time between 6.4 ka and present (Adams et al., 2022; Balco et al., 2023). A discordant initial in situ $^{14}$C age for CIN-112 (3.4 ± 0.3 ka, 179 m a. s. l.) younger than the $^{10}$Be exposure age (6.6 ± 0.4) from the same sample and other higher elevation in situ $^{14}$C ages from scoria cone supports such burial occurring during the late Holocene. The in situ $^{14}$C replicate measurement, CIN-112-R, however, yields an exposure age of 7.2 ± 0.9 ka, in agreement with the existing $^{10}$Be age. Both in situ $^{14}$C exposure ages determined from measurements of sample CIN-108 (collected from the same outcrop and elevation as CIN-112) are early-mid Holocene (CIN-108 – 6.3 ± 0.7 ka; CIN-108-R – 7.8 ± 1.0 ka). With the exception of the initial $^{14}$C exposure age from sample CIN-112, all exposure ages from the lower scoria cone outcrop (Adams et al., 2022) suggest that ice cover during the late Holocene was short-lived.

At both Turtle Rock and Notebook Cliffs, there is little evidence to suggest prolonged cover or burial of samples. At Turtle Rock, discordant $^{14}$C-$^{10}$Be exposure ages of TUR-117 and TUR-123 could be due to individual samples being partially shielded by till or ice debris cover during the Holocene, but the preferential sampling of topographic highs makes this less likely (Johnson et al., 2020). Furthermore, the in situ $^{14}$C exposure age of TUR-117-R (8.2 ± 1.1 ka) agrees with the existing $^{10}$Be exposure age at the site. There is no geological explanation for the same nuclide (in situ $^{14}$C) measured on the same sample (TUR-117) yielding two different in situ $^{14}$C exposure ages.

At Notebook Cliffs all $^{14}$C exposure ages (n = 3) are late Holocene and discordant with existing $^{10}$Be ages, implying inheritance in $^{10}$Be and prolonged burial of all three samples. The three Notebook Cliffs in situ $^{14}$C exposure ages contradict evidence from lower elevations of Mt Murphy that indicate early to mid-Holocene deglaciation from 9–6 ka (Johnson et al., 2020; Adams et al., 2022; Balco et al., 2023). In situ $^{14}$C ages from Notebook Cliffs could be reconciled with the currently accepted Mt Murphy deglaciation history if a localised ice dome had persisted atop Notebook Cliffs, shielding samples until the late Holocene. The flat top of the Notebook Cliffs site would favour persistence of a post-glacial ice dome; however, there is no physical evidence for this having occurred (Johnson et al., 2020). The difference in discordant in situ $^{14}$C concentrations (CIN-112, TUR-117) and replicate measurements from Turtle Rock and scoria cone (CIN-112-R, TUR-117-R) imply, however, that repeat in situ $^{14}$C measurement from Notebook Cliffs may have been in closer agreement with the Notebook Cliff $^{10}$Be exposure ages. In summary, evidence for

https://doi.org/10.5194/gchron-2024-34
Preprint. Discussion started: 9 December 2024


localised geological and topographical drivers of repeated burial and exposure of samples at Mt Murphy are currently lacking, with the exception of late Holocene ice cover of samples CIN-108 and CIN-112 at the lower scoria cone outcrop.

#### 4.2.1 Comparisons of the Mt Murphy and Shark Fin nunatak paired in situ $^{14}$C-$^{10}$Be datasets

The $^{14}$C-$^{10}$Be paired exposure age dataset from Shark Fin Nunatak adjacent to Tucker Glacier in the Ross Sea Embayment (Fig. 7) shares many similarities with the new Mt Murphy dataset. At Shark Fin Nunatak, Balco et al. (2019) explain the range of concordant and discordant paired in situ $^{14}$C-$^{10}$Be ages by samples of the same lithology having been initially exposed at higher elevations upstream for varying durations of time, subjecting them to a higher nuclide production rate. They postulate that exposed boulders then fell from cliffs and were transported supraglacially to their present position at Shark Fin nunatak. The suggestion of prior exposure followed by supraglacial transport is supported by evidence of extensive weathering of many of the Shark Fin samples. An upstream, higher elevation origin is also highly plausible due to the alpine setting of both Tucker Glacier and its tributary, Whitehall Glacier (Fig. 10b).

The overall conclusion at Shark Fin nunatak was that the youngest and discordant in situ $^{14}$C ages reflect the most straightforward and probable exposure history, while concordant in situ $^{14}$C-$^{10}$Be samples must have been subject to varying amounts of inheritance (Balco et al., 2019). The majority of $^{10}$Be exposure ages, and a few paired $^{14}$C ages range between 20–30 ka, precede the Holocene, which suggests that those samples have varying amounts of $^{10}$Be and in situ $^{14}$C inheritance. It should be noted that, at Shark Fin nunatak, both the in situ $^{14}$C ages and $^{10}$Be ages are older than Holocene age, whereas at Mt Murphy all paired $^{14}$C-$^{10}$Be exposure ages being examined are Holocene.

There are very few areas of exposed bedrock immediately upstream of Mt Murphy (Fig. 10a), making a similar geological explanation for the distribution of paired $^{14}$C-$^{10}$Be exposure ages at Mt Murphy as at Shark Fin Nunatak problematic and unlikely. The only site with rock outcrop immediately upstream of Mt Murphy is Mt Takahe, but Mt Takahe does not possess the same lithology as erratic boulders observed at Mt Murphy e.g., aplite, granite, and gneiss (Johnson et al., 2020; Adams et al., 2022), and is instead composed of extrusive igneous rock (see online database for Ohio State Polar Rock Repository; https://prr.osu.edu/collection/ [web accessed - 15.02.2024]). The only area of exposed rock nearby where granite has been observed is the Kohler Range (Fig. 11, Fig. S6). However, the Kohler Range does not lie upstream of Mt Murphy in the present ice flow configuration (Fig. 11a). A radical past re-organisation of ice flow would be required for erratics to be transported to Mt Murphy from the Kohler Range, for which there is no post-LGM evidence. In addition, erratics of exotic lithology from Notebook Cliffs, Turtle Rock and scoria cone measured for both $^{14}$C and $^{10}$Be are much less heavily weathered than samples at Shark fin nunatak, and so could not be considered to have arrived at Mt Murphy via supraglacial transport (for further geological information on Mt Murphy samples see Supplement S1). In summary, Mt Murphy is a remote site, and erratics sampled here show little evidence of having been transported supraglacially from a higher elevation site upstream. Therefore, the existence of discordant and concordant $^{14}$C-$^{10}$Be ages cannot be explained geologically in the same way as they can at Shark Fin nunatak. Furthermore, at Mt Murphy, with the exception of the scoria cone, there is little evidence from local topography to explain concordant-discordant paired $^{14}$C-$^{10}$Be exposure ages, although there is room for speculation at higher elevation sites. Still, any geological justification no matter how

https://doi.org/10.5194/gchron-2024-34
Preprint. Discussion started: 9 December 2024


complex cannot explain irreproducible in situ $^{14}C$ exposure ages at multiple sites. Paired $^{14}C$-$^{10}Be$ exposure ages at Shark Fin nunatak (Fig. 8a) reflect the same patterns of concordance and discordance observed at Mt Murphy (Fig. 4). However, $^{14}C$-$^{10}Be$ ratios at Shark Fin nunatak (Fig. 8b) to a varying extent all suggest a simple exposure history whereas at Mt Murphy, samples exhibit simple, complex, and seemingly impermissible exposure histories (Fig. 5).

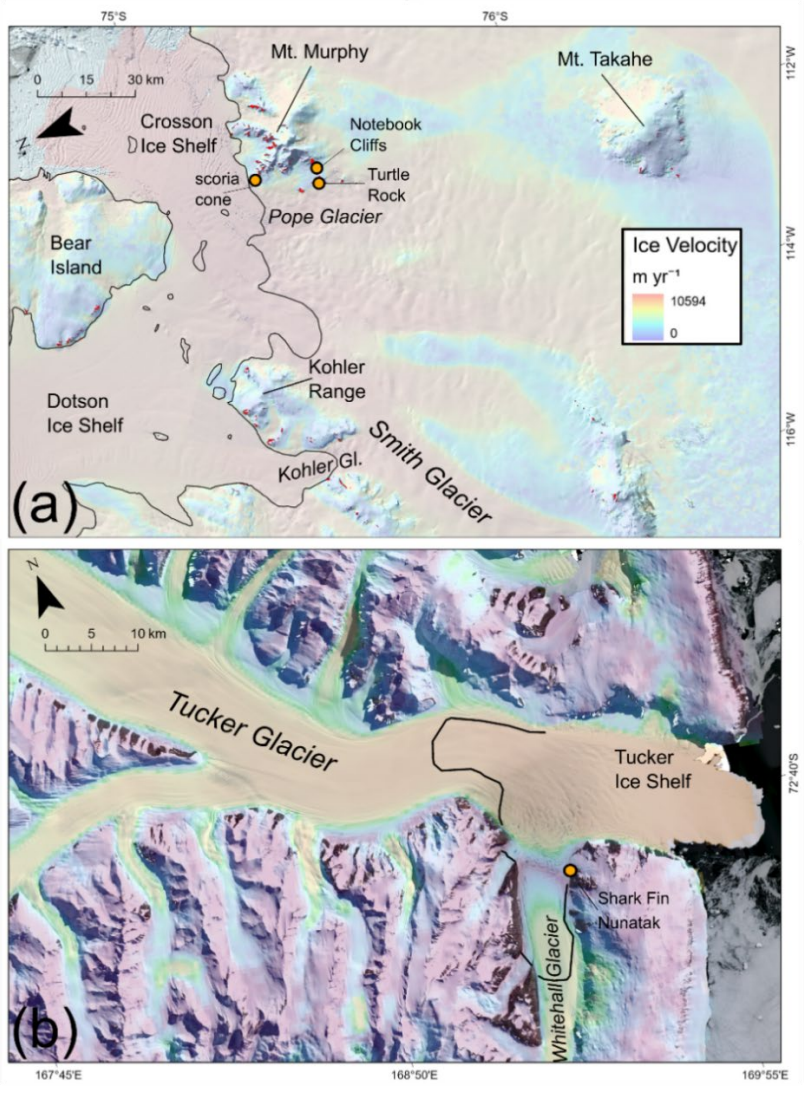


**Figure 10:** Regional comparison of Mt Murphy **(a)** and Tucker Glacier **(b)** demonstrating the comparative topographic isolation of Mt Murphy compared to Tucker Glacier. Orange circles show paired $^{14}C$-$^{10}Be$ sample sites mentioned in the text. Black lines in both images show locations of grounding lines determined by differential satellite radar interferometry (Rignot et al., 2011a). Ice flow speeds are displayed to improve visualisation of ice streams and were downloaded from MEaSUREs InSAR-Based Antarctica Ice Velocity dataset Version 2 (Mouginot et al., 2012, 2017; Rignot et al., 2011b) [last accessed 25.05.2023]. To improve visualisation exposed rock outcrops in Panel **(a)** are displayed red using the Antarctic rock outcrop dataset (Burton-Johnson et al., 2016). Both satellite images are sourced from Landsat Image Mosaic of Antarctica (LIMA; lima.usgs.gov).

https://doi.org/10.5194/gchron-2024-34
Preprint. Discussion started: 9 December 2024


### 4.3 Discussion of $^{14}C$-$^{10}Be$ endmember datasets from ICE-D analysis

In this section, we further contextualise Mt Murphy paired $^{14}C$-$^{10}Be$ concentration ratios by discussing the relevant background of existing datasets from Kangiata Nunata Sermia, Rhône Glacier and Sjögren Glacier, which display dominant Type-1, Type-2, and Type-3 nuclide concentration ratios, respectively.

The Type-1 endmember $^{14}C$-$^{10}Be$ dataset is from KNS, Greenland. The data exhibit concordant $^{14}C$-$^{10}Be$ exposure ages and $^{14}C$-$^{10}Be$ ratios consistent with a simple exposure history (Young et al., 2021). Observations from the KNS study site are well documented, both historically back to the 1850's (Young et al., 2021 cf. Fig. 10) and presently (Young et al., 2021 cf. Fig. 2). As a result, observational uncertainties are minimal, which permits the maximum permissible duration of Holocene exposure to be constrained, in this case to $^{10}Be$ of 10.20 ± 0.23 ka (Young et al., 2021). The study in which this dataset was generated benefitted from local production rate calibration datasets from West Greenland for $^{10}Be$ and in situ $^{14}C$ (Young et al., 2014), ensuring that production rates and the $^{14}C$-$^{10}Be$ production ratio were regionally constrained (Young et al., 2021). Finally, sources of analytical uncertainty of in situ $^{14}C$ were propagated for each sample based on long-term CRONUS-A measurements from the Lamont Doherty Earth Observatory where extraction took place (Lamp et al., 2019). All six samples without $^{10}Be$ inheritance possess $^{14}C$-$^{10}Be$ ratios that are indistinguishable and therefore imply a simple exposure history. In terms of accuracy, the $^{10}Be$ ages obtained from KNS are confirmed by concordant $^{14}C$ ages. The Type-1 dataset from KNS is associated with well constrained concordant paired $^{14}C$-$^{10}Be$ exposure ages that permit the Holocene deglaciation history of the site to be reconstructed with high confidence. From the filter analysis of ICE-D, eight other sites display $^{14}C$-$^{10}Be$ concentration ratios that are exclusively Type-1: Mario Zuchelli Station and Cape Marsh-Robertson Island from Antarctica (Jeong et al., 2018; Goehring et al., 2019b) and six sites from elsewhere around the globe (see Table 2). However, five of these eight sites all contain only one $^{14}C$-$^{10}Be$ pair each, which were extracted based on the Holocene search filter.

The Type-2 endmember dataset is taken from the Rhône Glacier exposure age dataset from the Swiss Alps (Goehring et al., 2011). Notebook Cliffs appears to be the only other dataset that exclusively exhibits Type-2 $^{14}C$-$^{10}Be$ concentration ratios (Table 3). Much like paired $^{14}C$-$^{10}Be$ ratios from Notebook Cliffs and paired $^{14}C$-$^{10}Be$ ratios based on the initial in situ $^{14}C$ measurements of TUR-117 and CIN-112 (Fig. 5a), the $^{14}C$-$^{10}Be$ ratios from Rhône Glacier plot within the area of complex exposure. The Rhône Glacier study effectively utilised the complex exposure and burial history of the samples uncovered from the forefield of the glacier to determine when it likely expanded and contracted during the Holocene (Goehring et al., 2011). Historical records aid with the interpretation of Rhône Glacier exposure ages (much like at KNS) as the samples are known to have been covered in the recent past when the glacier expanded during the Little Ice Age (Goehring et al., 2011). The Rhône Glacier dataset is more straightforward to interpret than the Mt Murphy dataset because all $^{14}C$-$^{10}Be$ exposure age pairs (except one outlier) plot below the steady erosion line. At Mt Murphy, apparent discordant and concordant $^{14}C$-$^{10}Be$ paired exposure ages from the same elevation suggest that some, but not all, samples were shielded during the Holocene, requiring a complex geologic model. The model used to explain exposure ages at Shark Fin Nunatak, however, cannot be applied to Mt Murphy (see Sect. 4.2), and so the cause of Type-2 $^{14}C$-$^{10}Be$ ratios at Mt Murphy currently lacks a coherent geological explanation.

https://doi.org/10.5194/gchron-2024-34
Preprint. Discussion started: 9 December 2024


The Type-3 endmember dataset from Sjögren Glacier - Site C (Balco and Schaefer, 2013) displays impermissible $^{14}C$-$^{10}Be$ concentration ratios (when assuming a constant surface production rate). At Mt Murphy, no samples have impermissible $^{14}C$-$^{10}Be$ ratios, but TUR-138 almost plots above the constant exposure line, and CIN-102 and TUR-132 also display high $^{14}C$-$^{10}Be$ ratios (Fig. 4). Exposure ages from Sjögren Glacier samples are bimodal. One group of mid-Holocene exposure ages (including replicates) decreases in age with elevation, from 4.8 ka at 120 m a. s. l. to 3.4 ka at 40 m a. s. l., whilst some samples suggest extremely recent exposure between just 200–500 years ago (Balco and Schaefer, 2013). From analysis of $^{10}Be$ ages, it was suggested that the site was fully deglaciated at 3.5–4.5 ka, partially covered again by thickening of the adjacent Boydell Glacier at or after ca 1.4 ka, and then deglaciated again between 1969 and the present (Balco and Schaefer, 2013). A complex exposure scenario at Sjögren Glacier may have, therefore, created specific conditions in which seemingly implausible $^{14}C$-$^{10}Be$ ratios can be explained geologically if samples at Sjögren Glacier-Site C were buried under a thin layer of cold-based ice during the Holocene, prior to more recent exposure. An impermissible $^{14}C$-$^{10}Be$ concentration ratio (when assuming surface production) could therefore become plausible if samples at Sjögren Glacier were subject to long periods of subsurface production during the Holocene or recent rapid exhumation from moderate depth (Rand and Goehring, 2019).

### 4.4 Investigating the effect of subsurface production by muons on $^{14}C$-$^{10}Be$ ratios

We now evaluate results of modelling high in situ $^{14}C$ relative to $^{10}Be$ production in the subsurface and explore if this can lead to a plausible geological explanation of the Sjögren Glacier Type-3 dataset. Two scenarios were modelled where an offset in situ $^{14}C$ relative to $^{10}Be$ production by muons could lead to high impermissible $^{14}C$-$^{10}Be$ concentration ratios at Sjögren Glacier: 1) An increase in erosion rate and 2) a duration of burial of a sample at shallow to moderate depth (1–5 metres) in the subsurface. Type-3 $^{14}C$-$^{10}Be$ ratios observed at Sjögren Glacier, however, could not be reconciled by modelling faster erosion rates (a faster rate of ice surface thinning) or prolonged burial under a thin layer of ice.

Increasing ice surface thinning (erosion rates) above 300–400 mm $kyr^{-1}$ leads to resulting modelled in situ $^{14}C$-$^{10}Be$ nuclide concentration ratios plotting above the constant exposure line, but only when $^{10}Be$ concentrations are low (see Fig. 9a). None of the Sjögren Glacier samples, however, exhibit low $^{10}Be$ nuclide concentrations (range; 18070 ± 591 to 27670 ± 686 at $g^{-1}$). The surface nuclide concentration is inversely proportional to the erosion rate, meaning there is an intersection between maximising the duration of greater $^{14}C$ production over an integrated depth and minimising the impact of the faster rate of decay of $^{14}C$ relative to $^{10}Be$. Consequently, high $^{14}C$-$^{10}Be$ ratios are only permitted when $^{10}Be$ concentration in a sample is low, due to the increasingly fast removal of accumulated nuclides at higher erosion rates.

Modelling prolonged burial of a sample at depths greater than ~ 2.5–3 metres under ice leads to high $^{14}C$-$^{10}Be$ ratios comparable to $^{14}C$-$^{10}Be$ ratios of Sjögren Glacier samples (Fig. 9b). The high $^{14}C$-$^{10}Be$ production ratio at depth is due to the almost complete attenuation of the high energy neutron flux (Dunai, 2010), and dominance of nuclide production due to negative muon capture (Heisinger et al., 2002; Balco, 2017). However, high $^{14}C$-$^{10}Be$ ratios are again only observed when the $^{10}Be$ concentration is low (< 1000 at $g^{-1}$). Over longer burial durations where greater concentrations of $^{10}Be$ accumulate, the high in situ $^{14}C$ to $^{10}Be$ production ratio is offset by the much faster decay rate of in situ $^{14}C$ relative to $^{10}Be$. In addition, the likely exposure history at

https://doi.org/10.5194/gchron-2024-34
Preprint. Discussion started: 9 December 2024


Sjögren Glacier, Site C indicated from $^{10}$Be ages is 2-3 kyr of initial surface exposure followed by shallow burial under a thin ice layer at 1.4 ka (Balco and Schaefer, 2013). In this case, the significant duration of surface exposure precludes the high $^{14}$C-$^{10}$Be concentration ratios observed in the Sjögren Glacier samples, due to the significant quantities of in situ $^{14}$C and $^{10}$Be atoms already accumulated in the sample at the surface production ratio.

In summary, observed ratios of $^{14}$C-$^{10}$Be relative to $^{10}$Be concentrations at Sjögren Glacier cannot be reconciled by either faster erosion (ice surface thinning) rates or prolonged burial at shallow to moderate ice thicknesses (1–5 metres). In both scenarios, if the concentration of $^{10}$Be atoms is low, high modelled $^{14}$C-$^{10}$Be ratios comparable to the $^{14}$C-$^{10}$Be concentration ratios in Sjogren Glacier samples are observed. However, as soon as $^{10}$Be nuclide concentrations exceed 1000–2000 atoms g$^{-1}$, high $^{14}$C-$^{10}$Be ratios are no longer observed due to 1) high erosion rates rapidly removing accumulated nuclides and or 2) the more rapid decay of in situ $^{14}$C relative to $^{10}$Be offsetting the higher $^{14}$C-$^{10}$Be subsurface production ratio. All measured in situ $^{14}$C nuclide concentrations from Sjögren Glacier Site C also appear to be systematically offset by approximately 5000 extra $^{14}$C atoms, suggesting a potential contaminant source of in situ $^{14}$C to these samples. A high proportion of samples from Sjögren Glacier Site C are vein quartz (see Table S3), which has previously been speculated to impact in situ $^{14}$C extraction due to the frequent presence of fluid inclusions (Nichols et al., 2019). Therefore, it is possible Type-3 ratios observed at Sjögren Glacier are due to an additional carbon source present in the quartz or incorporated during in situ $^{14}$C extraction.

### 4.5 Assessing the reproducibility of in situ $^{14}$C

We now evaluate in situ $^{14}$C reproducibility determined from the results of Mt Murphy replicate sample measurements and the wider ICE-D database. In this study only 1 of 4 of the Mt Murphy replicate in situ $^{14}$C measurements reproduced using a 6% 1σ measurement uncertainty. The Mt Murphy replicates contribute to a total of 18 of the 31 samples extracted from ICE-D where one or more replicates measurements do not reproduce within the nominal 1 σ 6 % analytical uncertainty based on repeat measurements of CRONUS-A at Tulane Laboratory (Goehring et al., 2019a). Many replicate measurements included in the ICE-D Holocene filter analysis are from Sjögren and Drygalski Glaciers (n = 5), sites which also yielded many impermissible paired $^{14}$C-$^{10}$Be ratios (Fig. 7). Results from the ICE-D filter of reproducibility (Fig. 10), therefore, suggest a possible link between in situ $^{14}$C reproducibility and Type-3 $^{14}$C-$^{10}$Be concentration ratios. The lack of an apparent geologic explanation for repeat in situ $^{14}$C measurements from field samples not reproducing within 1 σ 6 % analytical uncertainties suggests that sample preparation uncertainty estimation may be too low. We therefore investigate in situ $^{14}$C reproducibility by examining CRONUS-A reproducibility and in situ $^{14}$C process blank values (Table 3).

#### 4.5.1 Sources of uncertainty affecting in situ $^{14}$C reproducibility – CRONUS-A

In situ $^{14}$C concentrations for CRONUS-A reported from extraction facilities range from 6.12 ± 0.32 x 10$^5$ at g$^{-1}$ (Goehring et al., 2019a) to 7.28 ± 0.03 x 10$^5$ at g$^{-1}$ (Lupker et al., 2019). The CRONUS-A value reported from Tulane is 5–10 % lower than other in situ $^{14}$C extraction laboratories and below the "consensus" interlaboratory value (n = 23) of 6.97 x 10$^5$ atoms g$^{-1}$ of Jull et al. (2015). Interlaboratory comparison of CRONUS-A in situ $^{14}$C values therefore suggest a 6 % measurement uncertainty is too

https://doi.org/10.5194/gchron-2024-34
Preprint. Discussion started: 9 December 2024


low (Jull et al., 2015). LDEO report a higher than average in situ $^{14}C$ concentration for CRONUS-A of 7.18 ± 0.15 x $10^5$ atoms $g^{-1}$ (Lamp et al., 2019), making the CRONUS-A value reported from Tulane 14.8 % lower than the value reported from LDEO. The difference between CRONUS-A values reported by Tulane and LDEO, however, explains why the $^{14}C$-$^{10}Be$ ratio from sample TUR-138, (extracted at LDEO) plotted above the constant exposure line (Fig. 5a, Fig. 7a). Reducing the in situ $^{14}C$ concentration of TUR-138 by 14.8 % from 2.03 x $10^5$ at $g^{-1}$ to 1.73 x $10^5$ at $g^{-1}$ results in TUR-138 plotting within the steady-state erosion island.

**Table 3:** Summary table of CRONUS-A intercomparison material and long-term blank values reported from different in situ $^{14}C$ extraction facilities. Note – Tulane and LDEO are examined more closely over several measurement cycles as in situ $^{14}C$ measured from Mt Murphy samples was extracted at both facilities. The latest AixMICADAS gas ion source AMS measurements reported by LDEO are also included to highlight improved $^{14}C$ background levels using this extraction technique. *In Balco et al., (2022) long-term blank values for Tulane surface sample measurements presented in this study are not reported but blank variability at Tulane over this time period is discussed at length.

| Extraction Laboratory | CRONUS A (at $g^{-1}$) | No. CRONUS-A | Long-term blank (at $g^{-1}$) | Associated Publication |
|---|---|---|---|---|
| Tulane - pre-2019 | 6.12 ± 0.32 x $10^5$ | 10 | 0.98 ± 0.32 x $10^5$ | Goehring et al., 2019 |
| Tulane - Mt Murphy (initial) | 6.12 ± 0.32 x $10^5$ | | 4.53 ± 0.24 x $10^4$ | *Balco et al., 2022 |
| Tulane - Mt Murphy (replicates) | 6.12 ± 0.32 x $10^5$ | | 7.14 ± 0.30 x $10^4$ | *Balco et al., 2022 |
| LDEO - Graphitised pre-2014 | 6.74 ± 0.10 x $10^5$ | 5 | 1.19 ± 0.37 x $10^5$ | Lamp et al., 2019 |
| LDEO - Graphitised post-2014 | 7.18 ± 0.15 x $10^5$ | 7 | 1.19 ± 0.37 x $10^5$ | Lamp et al., 2019 |
| LDEO - AixMICADAS | 6.62 ± 0.09 x $10^5$ | 5 | 0.75 ± 0.04 x $10^5$ | Young et al., 2021 |
| ETH Zurich (2011 - 2013) | 7.09 ± 0.39 x $10^5$ | 13 | 3.48 ± 2.04 x $10^4$ | Lupker et al., 2015 |
| ETH Zurich 2018 | 7.28 ± 0.03 x $10^5$ | 7 | 2.63 ± 1.05 x $10^5$ | Lupker et al., 2019 |
| Cologne | 6.72 ± 0.71 x $10^5$ | 6 | 1.00 ± 0.68 x $10^4$ | Fulop et al., 2015 |
| ANSTO | 6.93 ± 0.44 x $10^5$ | 14 | 0.98 ± 0.68 x $10^4$ | Fulop et al., 2019 |
| PRIME Lab (Purdue) | 6.89 ± 0.04 x $10^5$ | 6 | 1.84 ± 0.38 x $10^5$ | Lifton et al., 2015 |
| University of Arizona | 7.08 ± 0.17 x $10^5$ | 12 | 3.40 ± 0.90 x $10^4$ | Lifton et al., 2023 |
| Working interlaboratory - Mean | 6.93 ± 0.44 x $10^5$ | 23 | | Jull et al., 2015 |
| Working interlaboratory - Median | 6.97 x $10^5$ | 23 | | Jull et al., 2015 |

Inconsistencies in the interlaboratory reproducibility of CRONUS-A and corresponding underestimation of in situ $^{14}C$ measurement uncertainty has been documented in previous studies highlighting that laboratories uniformly underestimated the magnitude by which empirical coefficients of variation exceeded average reported analytical uncertainties for all nuclides (Phillips et al., 2016a; Jull et al., 2015). However, the underestimation in the reported analytical uncertainty exceeds 300 % for $^{14}C$ on the CRONUS-A material (Phillips et al., 2016b). Moreover, in an effort to calibrate in situ $^{14}C$ spallogenic production, Borchers et al. (2016) found that scatter of in situ $^{14}C$ measurements in excess of an assumed uncertainty of 7.3 % was more significant than variability between production rate calibration sites (Borchers et al., 2016). Impurities in quartz mineral separates have previously been evidenced to

https://doi.org/10.5194/gchron-2024-34
Preprint. Discussion started: 9 December 2024


negatively impact the reproducibility of $^{10}$Be (Corbett et al., 2022), and it is possible quartz impurities are also contributing to the lack of in situ $^{14}$C reproducibility in our Mt Murphy dataset. However, a preliminary investigation based on ICP-EOS elemental data of Mt Murphy samples measured for in situ $^{14}$C in this study found no significant link between low abundances of elemental impurities in quartz mineral separates and in situ $^{14}$C reproducibility (see Supplement S3, Table S4, Table S5).

The CRONUS-A intercomparison material is derived from a high elevation site (1612 m) in Antarctica with millions of years of constant exposure, making it saturated with respect to $^{14}$C (mean value = 6.93 ± 0.44 x $10^5$, Jull et al., 2015). Reproducibility estimates from CRONUS-A are, therefore, only representative for high concentration samples, for which AMS counting errors and blank contributions are typically low (Hippe, 2017). Achieving the same level of measurement precision in a sample with a lower concentration of in situ $^{14}$C in a sample is more challenging, and a typical sample exposed during the Holocene will yield an in situ $^{14}$C concentration lower than CRONUS-A. For instance, sample 10-MPS-022-CSP from the Schmidt Hills (8.3 ± 0.8 ka, 352 m a. s. l.) has an in situ $^{14}$C concentration of 1.28 ± 0.20 $10^5$ at $g^{-1}$ (Nichols et al., 2019). Samples exposed during the Holocene, and particularly those at low elevations such as the scoria cone and Kay Peak, are therefore more sensitive to blank correction than CRONUS-A.

#### 4.5.2 Assessing uncertainty affecting in situ $^{14}$C reproducibility – in situ $^{14}$C blank measurements

For our samples, the blank correction applied to in situ $^{14}$C repeat measurements was higher than that of the initial $^{14}$C measurements (see Table 3). We also assigned a nominal 6 % 1σ measurement uncertainty to in situ $^{14}$C concentrations in this study which assumes scatter in process blank concentrations was normally distributed (Goehring et al., 2019a). The distribution of the long-term $^{14}$C measurement background of samples from the Tulane University extraction facility over which our initial and replicate samples were measured in this study is, however, long-tailed and non-time dependent (Balco et al., 2022).

Blank correction of in situ $^{14}$C AMS measurements using a long-tailed distribution is appropriate for low concentration samples such as subglacial bedrock cores (Balco et al., 2023) for which blank variability constitutes the dominant source of uncertainty in the in situ $^{14}$C measurements (Balco et al., 2022). Applying this same blank correction (assuming a long-tailed distribution) to in situ $^{14}$C concentrations measured in our Mt Murphy surface samples results in 2 of 4 in situ $^{14}$C replicate samples reproducing at 68 % confidence. In addition, the exposure age calculated from the in situ $^{14}$C concentration CIN-108-R becomes concordant with the CIN-108 $^{10}$Be exposure age (68 % confidence). However, uncertainty ranges in Mt Murphy surface sample concentrations are very large when using the long tailed blank correction (see Fig. S8), especially for the replicates reported with a higher blank (7.14 ± 0.30 x $10^5$ $^{14}$C atoms $g^{-1}$). For instance, the 68 % confidence uncertainty estimate for the in situ $^{14}$C concentration of CIN-112-R is +24.1 %, -11.2%, which when propagated results in an uncertainty on the exposure age of CIN-112-R of > 4 kyr.

The differences in in situ concentrations and replicate in situ $^{14}$C concentrations may be explained, in part, by several changes made to the in situ $^{14}$C extraction line at Tulane between the extraction of in situ $^{14}$C for the initial and replicate measurements, including the addition of a new coil trap (Lifton et al., 2023) and a new mullite tube which has previously been observed to increase background $^{14}$C (see methods section 2.1). It is not clear how significant the high blank may have been to the final measurements, or if it represents a systematic addition of in situ $^{14}$C to the replicate in situ $^{14}$C exposure ages. It does, however,

https://doi.org/10.5194/gchron-2024-34
Preprint. Discussion started: 9 December 2024


reiterate the importance of minimising blank levels, and potentially suggests that the long-tailed blank correction discussed at length in Balco et al., (2022) should be applied to in situ $^{14}C$ measurements, especially for samples such as those in bedrock cores and our Mt Murphy surface samples.

### 4.5.3 Reducing in situ $^{14}C$ background – gas-ion source AMS of non-graphitised in situ $^{14}C$ samples

Directly measuring $CO_2$ has the potential to lower the blank value as it removes a source of in situ $^{14}C$ background contribution from graphitisation (Hippe et al., 2013; Bard et al., 2015). The LDEO extraction facility noted improved procedural blanks by measuring situ $^{14}C$ using the AixMICADAS gas-ion source AMS instrument, reporting a 35 % reduction in the average in situ $^{14}C$ blank concentration from 1.19 ± 0.37 x $10^5$ atoms $g^{-1}$ $^{14}C$ to 0.75 ± 0.04 x $10^5$ atoms $g^{-1}$ $^{14}C$ (Lamp et al., 2019). AMS measurements also yielded a lower CRONUS-A concentration of 6.59 ± 0.09 x $10^5$ atoms $g^{-1}$ $^{14}C$ (Lamp et al., 2019), much closer to CRONUS-A measurements reported from Tulane (difference < 6000 atoms $g^{-1}$). The lower CRONUS-A in situ $^{14}C$ concentration and reduced background using AixMICADAS may suggest a source of contaminant $^{14}C$ impacted earlier CRONUS-A extraction at LDEO (Lamp et al., 2019; Young et al., 2021). Notably, in situ $^{14}C$ CRONUS-A samples extracted at LDEO and measured using the AixMICADAS gas ion source AMS are now much closer to long-term CRONUS-A values reported from Tulane. Blanks also seem to be an order of magnitude lower (1-4 x $10^4$ at $g^{-1}$) for extraction lines where sample combustion is performed without $LiBO_2$ flux (Hippe et al., 2013; Lupker et al., 2015; Fülöp et al., 2019), as opposed to flux-based systems (1–4 x $10^5$ at $g^{-1}$) (Pigati et al., 2010; Goehring et al., 2014; Lifton et al., 2015b). Mean blank values from systems not using $LiBO_2$ flux are though subject to larger uncertainties ranging from 60–160 % (1 σ), reflecting the large scatter in the blank data (Hippe, 2017).

More recent in situ $^{14}C$ measurements performed on the AixMICADAS AMS yield a mean CRONUS-A value of 6.62 ± 0.09 x $10^5$ atoms $g^{-1}$ (n = 5) (Young et al., 2021). Notably, 10 of 12 in situ $^{14}C$ exposure ages reported in Young et al. (2021) which make up the $^{14}C$-$^{10}Be$ paired exposure ages from Kangiata Nunaata Sermia (KNS), were measured using the AixMICADAS gas ion source AMS in concert with the LDEO CRONUS-A samples reported above. Concordant $^{14}C$-$^{10}Be$ exposure ages and Type-1 $^{14}C$-$^{10}Be$ ratios from KNS all suggest a simple exposure history (Young et al., 2021). In this case, the removal of potentially contaminant sources of in situ $^{14}C$ from the extraction process (Young et al., 2021) has coincided with the generation of $^{14}C$ exposure ages, which are both accurate and consistent with paired $^{10}Be$ measurements from the same sample (Fig. 7b). The two graphitised samples measured at LLNL-CAMS have uncertainties that are 7.7 % and 10.4 %, in contrast to samples measured using a gas ion source at CEREGE, where total $^{14}C$ concentration uncertainties ranged from 4.3 % to 5.2 % (Young et al., 2021). We do note, however, that in situ $^{14}C$ measurements of all five graphitised samples from Promontory Point, Lake Bonneville (Lifton et al., 2015a) largely agree within 6 % 1σ analytical uncertainties (Fig. 10, Table S3). The CoV for Promontory Point samples is also 4.7 % (Lifton et al., 2015a), which is better than the CRONUS-A intercomparison CoV of 6.3 % reported by Jull et al. (2015). Therefore, we acknowledge that graphitisation of samples, can produce results comparable in quality to non-graphitised samples, but that graphitisation itself presents a potential source of uncertainty that can be avoided.

https://doi.org/10.5194/gchron-2024-34
Preprint. Discussion started: 9 December 2024


### 4.6 Summary and suggestions for future work

The findings presented in this paper suggest that stated laboratory uncertainties underestimate the true measurement uncertainty of in situ $^{14}C$. This is consistent with previous findings from the CRONUS-Earth Project (Phillips et al., 2016b; Borchers et al., 2016). The current interlaboratory variation in reported CRONUS-A in situ $^{14}C$ concentrations of ~ 15 % and in situ $^{14}C$ blank variability are highlighted as issues impacting the accuracy and precision of in situ $^{14}C$ measurements, as they have been previously (Hippe, 2017; Jull et al., 2015; Phillips et al., 2016a). We suggest that a new blank correction approach using a long-tailed blank distribution (Balco et al., 2022, 2023) may better account for the true analytical uncertainty in $^{14}C$ measurements, especially at low concentrations. The blank correction results in larger uncertainties on in situ $^{14}C$ concentrations, allowing for greater measurement scatter, and thereby improving measurement reproducibility. Ongoing progress including automation of in situ $^{14}C$ extraction (Goehring et al., 2019a; Lupker et al., 2019; Lifton et al., 2023) will help facilitate analysis of additional replicates and process blanks, which is needed to improve the precision of in situ $^{14}C$ measurements. With a focus on improving $^{14}C$ analytical reproducibility and precision, we therefore make the following suggestions which will ultimately contribute to the provision of robust combined $^{14}C$-$^{10}Be$ chronologies:

- Routinely undertaking and reporting more in situ $^{14}C$ replicate measurements. This will provide a check on quality control.
- Adopting the blank correction procedure outlined in Balco et al. (2023) for low concentration samples where blank scatter is dominant and blanks do not exhibit a normal distribution. This will provide a better appreciation of the true analytical long-tailed uncertainty distribution present in in situ $^{14}C$ measurements.
- Undertaking a comparison study of the reproducibility of graphitised versus non graphitised in situ $^{14}C$ measurements of the same sample(s) and associated blank performance.
- Quantifying if quartz impurities are contributing to poor reproducibility, in a more in-depth study similar to Corbett et al., (2022).

## 5 Conclusion

In this study, we have assessed new $^{14}C$-$^{10}Be$ exposure ages from Mt Murphy, West Antarctica, in the context of a wider repository of global Holocene age $^{14}C$-$^{10}Be$ paired measurements extracted from the informal cosmogenic-nuclide exposure age database (ICE-D, https://version2.ice-d.org/). New paired $^{14}C$-$^{10}Be$ exposure ages from several sites at Mt Murphy display conflicting exposure histories. Young in situ $^{14}C$ ages from high elevations that are discordant with $^{10}Be$ measured in the same sample appear to have deglaciated after concordant paired $^{14}C$-$^{10}Be$ exposure ages from lower elevations with simple exposure histories. Statistical analysis of a large in situ $^{14}C$ exposure age dataset (n = 20) from Mt Murphy also indicates scatter in excess of analytical uncertainty of almost 2 kyr. There is no apparent geological explanation for divergent concordant-discordant exposure histories nor excess scatter observed within the in situ $^{14}C$ dataset. Instead, we find that 3 of 4 replicate in situ $^{14}C$ measurements performed on samples from Mt Murphy do not reproduce within a 6 % 1σ measurement uncertainty, with 2 of 4 measurements still

https://doi.org/10.5194/gchron-2024-34
Preprint. Discussion started: 9 December 2024


not reproducing at 2σ. Furthermore, concordant $^{14}C$-$^{10}Be$ pairs at Mt Murphy with simple exposure histories exhibit reproducible in situ $^{14}C$ concentrations, but discordant in situ $^{14}C$ exposure ages suggestive of complex exposure are not reproducible. Our observations from Mt Murphy are reflected in reported in situ $^{14}C$ concentrations from ICE-D, where replicate in situ $^{14}C$ concentrations measured in 18 of 31 samples fail to reproduce within the 6 % 1σ measurement uncertainty (15 of 31 at 2σ) one or more times. In addition, Sjögren Glacier (a site where 2 of 3 replicate in situ $^{14}C$ concentrations are irreproducible) exhibits paired $^{14}C$-$^{10}Be$ production ratios which exceed theoretical limits and lack geological explanation.

In summary, the results of our analysis of $^{14}C$-$^{10}Be$ exposure ages from ICE-D are consistent with the interpretation that discordant $^{14}C$-$^{10}Be$ exposure ages from Mt Murphy are a result of isolated issues of in situ $^{14}C$ reproducibility, while concordant $^{14}C$-$^{10}Be$ pairs are consistent with a deglaciation history from 9–6 ka identified in previous studies. Currently, in situ $^{14}C$ measurement uncertainty may therefore be underestimated due to additional, as yet unquantified, sources of scatter. Several factors may contribute to the low in situ $^{14}C$ reproducibility observed in this study and require further investigation. These include long term blank variability within in situ $^{14}C$ extraction facilities, differences in CRONUS-A measurements between in situ $^{14}C$ extraction laboratories, and the influence of changes to the Tulane extraction line between in situ $^{14}C$ initial and replicate measurements. Quartz impurity may also impact sample reproducibility, although our preliminary examination of ICP-OES data found no evidence to suggest that quartz sample purity contributed to lack of in situ $^{14}C$ reproducibility in our samples. Quantifying the excess scatter observed in this study is important because, if used in isolation, in situ $^{14}C$ exposure ages appear to currently lack the precision needed to reconstruct Holocene deglacial histories at sub-millennial resolution.

https://doi.org/10.5194/gchron-2024-34
Preprint. Discussion started: 9 December 2024


**Data and code availability:** Some of the in situ $^{14}C$ data examined in this study were obtained from the informal cosmogenic-nuclide exposure age database (ICE-D) and remain unpublished. These data are, however, freely available in ICE-D under the public release requirements of the National Science Foundation (NSF) U.S. Antarctic Program which requires data be made publicly available 2 years after collection. In situ $^{14}C$ AMS and exposure age data shown in Table 1 will be publicly accessible in the UK Polar Data Centre https://doi.org/10.5285/dbb30962-bbf3-434a-9f27-6de2f61a86e2

**Author contribution**: The author contributions, following the CRediT authorship guidelines, are as follows – conceptualization: JRA, DHR, JSJ; methodology: JRA, DHR; validation: JRA, DHR; analysis: JRA, DHR; investigation: JRA, DHR, JSJ; resources: DHR, SJRO, JSJ: data curation: JRA, DHR; original draft: JRA, DHR; review and editing: JRA, DHR, KW, SJRO, JSJ: visualization: JRA; supervision: DHR, SJRO, JSJ; administration: JRA, DHR, JSJ; funding acquisition: DHR, JSJ.

**Competing interests**: The authors declare that they have no conflict of interest.

**Financial Support:** This research has been supported by the Natural Environment Research Council (grant nos. NE/S006710/1, NE/S006753/1, and NE/K012088/1) and National Science Foundation (grant: OPP-1738989).

**Acknowledgements**: This work is from the "Geological History Constraints" GHC project, a component of the International Thwaites Glacier Collaboration (ITGC). Support was from National Science Foundation (NSF: grant OPP-1738989) and Natural Environment Research Council (NERC: grant NE/S006710/1, NE/S006753/1, and NE/K012088/1). Logistics were provided by NSF-U.S. Antarctic Program and NERC-British Antarctic Survey**.** We acknowledge Mark Evans for assistance with rock sample preparation. We thank Ryan Venturelli and Brent Goehring for performing the in situ $^{14}C$ extractions at Tulane. In addition, we thank Greg Balco for assistance with subsurface in situ $^{14}C$-$^{10}Be$ production rate modelling and helpful advice on the manuscript. We also thank Keir Nichols for helpful advice on the manuscript. JRA would like to credit his PhD examiners Derek Fabel and Yves Plancherel for thoughtful and encouraging discussions regarding this research. This is ITGC contribution #XXX.

https://doi.org/10.5194/gchron-2024-34
Preprint. Discussion started: 9 December 2024




**References**

Adams, J. R., Johnson, J. S., Roberts, S. J., Mason, P. J., Nichols, K. A., Venturelli, R. A., Wilcken, K., Balco, G., Goehring, B., Hall, B., Woodward, J., and Rood, D. H.: New $^{10}$Be exposure ages improve Holocene ice sheet thinning history near the grounding line of Pope Glacier, Antarctica, Cryosph., 16, 4887–4905, https://doi.org/10.5194/tc-16-4887-2022, 2022.

Adams, J. R., Venturelli, R. A., Goehring, B. M., Johnson, J. S., Roberts, S. J., and Rood, D. H.: Cosmogenic in situ $^{14}$C data and calculated surface exposure ages for 9 erratic cobbles collected from Mount Murphy, West Antarctica, UK Polar Data Cent. [Dataset], https://doi.org/https://doi.org/10.5285/dbb30962-bbf3-434a-9f27-6de2f61a86e2, 2024.

Aerts-Bijma, A. T., Paul, D., Dee, M. W., Palstra, S. W. L., and Meijer, H. A. J.: An independent assessment of uncertainty for radiocarbon analysis with the new generation high-yield accelerator mass spectrometers, Radiocarbon, 63, 1–22, https://doi.org/10.1017/RDC.2020.101, 2021.

Argento, D. C., Stone, J. O., Reedy, R. C., and O'Brien, K.: Physics-based modeling of cosmogenic nuclides part I - Radiation transport methods and new insights, Quat. Geochronol., 26, 29–43, https://doi.org/10.1016/j.quageo.2014.09.004, 2015a.

Argento, D. C., Stone, J. O., Reedy, R. C., and O'Brien, K.: Physics-based modeling of cosmogenic nuclides part II - Key aspects of in-situ cosmogenic nuclide production, Quat. Geochronol., 26, 44–55, https://doi.org/10.1016/j.quageo.2014.09.005, 2015b.

Balco, G.: Contributions and unrealized potential contributions of cosmogenic-nuclide exposure dating to glacier chronology, 1990-2010, Quat. Sci. Rev., 30, 3–27, https://doi.org/10.1016/j.quascirev.2010.11.003, 2011.

Balco, G.: Production rate calculations for cosmic-ray-muon-produced $^{10}$Be and $^{26}$Al benchmarked against geological calibration data, https://doi.org/10.1016/j.quageo.2017.02.001, 1 April 2017.

Balco, G.: Glacier Change and Paleoclimate Applications of Cosmogenic-Nuclide Exposure Dating, Annu. Rev. Earth Planet. Sci., 48, https://doi.org/10.1146/annurev-earth-081619, 2020a.

Balco, G.: Technical note: A prototype transparent-middle-layer data management and analysis infrastructure for cosmogenic-nuclide exposure dating, 2, 169–175, https://doi.org/10.5194/GCHRON-2-169-2020, 2020b.

Balco, G. and Schaefer, J. M.: Exposure-age record of Holocene ice sheet and ice shelf change in the northeast Antarctic Peninsula, Quat. Sci. Rev., 59, 101–111, https://doi.org/10.1016/j.quascirev.2012.10.022, 2013.

Balco, G., Stone, J. O., Lifton, N. A., and Dunai, T. J.: A complete and easily accessible means of calculating surface exposure ages or erosion rates from $^{10}$Be and $^{26}$Al measurements, https://doi.org/10.1016/j.quageo.2007.12.001, August 2008.

Balco, G., Todd, C., Goehring, B. M., Moening-swanson, I., and Nichols, K.: Glacial geology and cosmogenic-nuclide exposure ages from the Tucker Glacier - Whitehall Glacier confluence, Northern Victoria Land, Antarctica, Am. J. Sci., 319, 255–286, https://doi.org/10.2475/04.2019.01, 2019.

Balco, G., Brown, N., Nichols, K., Venturelli, R. A., Adams, J., Braddock, S., Campbell, S., Goehring, B., Johnson, J. S., Rood, D.

https://doi.org/10.5194/gchron-2024-34
Preprint. Discussion started: 9 December 2024


H., Wilcken, K., Hall, B., and Woodward, J.: Response to review 2 (Nat Lifton) of "Reversible ice sheet thinning in the Amundsen Sea embayment during the late Holocene," Cryosph. Discuss., 33, 1–12, https://doi.org/doi.org/10.5194/tc-2022-172-AC2, 2022.

Balco, G., Brown, N., Nichols, K., Venturelli, R. A., Adams, J., Braddock, S., Campbell, S., Goehring, B., Johnson, J. S., Rood, D. H., Wilcken, K., Hall, B., and Woodward, J.: Reversible ice sheet thinning in the Amundsen Sea Embayment during the Late Holocene, Cryosph., 17, 1787–1801, 2023.

Bard, E., Tuna, T., Fagault, Y., Bonvalot, L., Wacker, L., Fahrni, S., and Synal, H. A.: AixMICADAS, the accelerator mass spectrometer dedicated to $^{14}C$ recently installed in Aix-en-Provence, France, Nucl. Instruments Methods Phys. Res. Sect. B Beam Interact. with Mater. Atoms, 361, 80–86, https://doi.org/10.1016/j.nimb.2015.01.075, 2015.

Binnie, S. A., Dewald, A., Heinze, S., Voronina, E., Hein, A., Wittmann, H., von Blanckenburg, F., Hetzel, R., Christl, M., Schaller, M., Léanni, L., ASTER Team, Hippe, K., Vockenhuber, C., Ivy-Ochs, S., Maden, C., Fülöp, R. H., Fink, D., Wilcken, K. M., Fujioka, T., Fabel, D., Freeman, S. P. H. T., Xu, S., Fifield, L. K., Akçar, N., Spiegel, C., and Dunai, T. J.: Preliminary results of CoQtz-N: A quartz reference material for terrestrial in-situ cosmogenic 10Be and 26Al measurements, Nucl. Instruments Methods Phys. Res. Sect. B Beam Interact. with Mater. Atoms, 456, 203–212, https://doi.org/10.1016/j.nimb.2019.04.073, 2019.

Borchers, B., Marrero, S., Balco, G., Caffee, M., Goehring, B., Lifton, N., Nishiizumi, K., Phillips, F., Schaefer, J., and Stone, J.: Geological calibration of spallation production rates in the CRONUS-Earth project, Quat. Geochronol., 31, 188–198, https://doi.org/10.1016/j.quageo.2015.01.009, 2016.

Briner, J. P., Lifton, N. A., Miller, G. H., Refsnider, K., Anderson, R., and Finkel, R.: Using in situ cosmogenic $^{10}Be$, $^{14}C$, and $^{26}Al$ to decipher the history of polythermal ice sheets on Baffin Island, Arctic Canada, Quat. Geochronol., 19, 4–13, https://doi.org/10.1016/j.quageo.2012.11.005, 2014.

Burton-Johnson, A., Black, M., Fretwell, P. T., and Kaluza-Gilbert, J.: An automated methodology for differentiating rock from snow, clouds and sea in Antarctica from Landsat 8 imagery: a new rock outcrop map and area estimation for the entire Antarctic continent, Cryosph., 10, 1665–1677, https://doi.org/10.5194/tc-10-1665-2016, 2016.

Corbett, L. B., Bierman, P. R., and Rood, D. H.: An approach for optimizing in situ cosmogenic $^{10}Be$ sample preparation, Quat. Geochronol., 33, 24–34, https://doi.org/10.1016/j.quageo.2016.02.001, 2016.

Corbett, L. B., Bierman, P. R., Brown, T. A., Caffee, M. W., Fink, D., Freeman, S. P. H. T., Hidy, A. J., Rood, D. H., Wilcken, K. M., and Woodruff, T. E.: Clean quartz matters for cosmogenic nuclide analyses: An exploration of the importance of sample purity using the CRONUS-N reference material, Quat. Geochronol., 73, 101403, https://doi.org/10.1016/j.quageo.2022.101403, 2022.

Dunai, T. J.: Cosmogenic nuclides: Principles, concepts and applications in the earth surface sciences, 1–187 pp., https://doi.org/10.1017/CBO9780511804519, 2010.

Fülöp, R., Wacker, L., and Dunai, T. J.: Progress report on a novel in situ $^{14}C$ extraction scheme at the University of Cologne, Nucl. Instruments Methods Phys. Res. B, 361, 20–24, https://doi.org/10.1016/j.nimb.2015.02.023, 2015.

https://doi.org/10.5194/gchron-2024-34
Preprint. Discussion started: 9 December 2024


Fülöp, R. H., Naysmith, P., Cook, G. T., Fabel, D., Xu, S., and Bishop, P.: Update on the performance of the suerc in situ $^{14}C$ extraction line, Radiocarbon, 52, 1288–1294, 2010.

Fülöp, R. H., Fink, D., Yang, B., Codilean, A. T., Smith, A., Wacker, L., Levchenko, V., and Dunai, T. J.: The ANSTO – University of Wollongong in-situ $^{14}C$ extraction laboratory, Nucl. Instruments Methods Phys. Res. Sect. B Beam Interact. with Mater. Atoms, 438, 207–213, https://doi.org/10.1016/J.NIMB.2018.04.018, 2019.

Goehring, B. M., Schaefer, J. M., Schluechter, C., Lifton, N. A., Finkel, R. C., Jull, A. J. T., Akçar, N., and Alley, R. B.: The Rhone Glacier was smaller than today for most of the Holocene, Geology, 39, 679–682, https://doi.org/10.1130/G32145.1, 2011.

Goehring, B. M., Schimmelpfennig, I., and Schaefer, J. M.: Capabilities of the lamont-doherty earth observatory in situ $^{14}C$ extraction laboratory updated, Quat. Geochronol., 19, 194–197, https://doi.org/10.1016/j.quageo.2013.01.004, 2014.

Goehring, B. M., Wilson, J., and Nichols, K.: A fully automated system for the extraction of in situ cosmogenic carbon-14 in the Tulane University cosmogenic nuclide laboratory, Nucl. Instruments Methods Phys. Res. Sect. B Beam Interact. with Mater. Atoms, 455, 284–292, https://doi.org/10.1016/j.nimb.2019.02.006, 2019a.

Goehring, B. M., Balco, G., Todd, C., Moening-Swanson, I., and Nichols, K.: Late-glacial grounding line retreat in the northern Ross Sea, Antarctica, Geology, 47, 291–294, https://doi.org/10.1130/G45413.1, 2019b.

Goehring, B. M., Menounos, B., Osborn, G., Hawkins, A., and Ward, B.: Reconciling the apparent absence of a Last Glacial Maximum alpine glacial advance, Yukon Territory, Canada, through cosmogenic beryllium-10 and carbon-14 measurements, 4, 311–322, https://doi.org/10.5194/gchron-4-311-2022, 2022.

Gosse, J. C. and Phillips, F. M.: Terrestrial in situ cosmogenic nuclides: Theory and application, Quat. Sci. Rev., 20, 1475–1560, https://doi.org/10.1016/S0277-3791(00)00171-2, 2001.

Granger, D. E.: A review of burial dating methods using $^{26}Al$ and $^{10}Be$, Spec. Pap. Geol. Soc. Am., 415, 1–16, https://doi.org/10.1130/2006.2415(01), 2006.

Hein, A. S., Fogwill, C. J., Sugden, D. E., and Xu, S.: Geological scatter of cosmogenic-nuclide exposure ages in the Shackleton Range, Antarctica: Implications for glacial history, Quat. Geochronol., 19, 52–66, https://doi.org/10.1016/j.quageo.2013.03.008, 2014.

Heisinger, B., Lal, D., Jull, A. J. T., Kubik, P., Ivy-Ochs, S., Knie, K., and Nolte, E.: Production of selected cosmogenic radionuclides by muons: 2. Capture of negative muons, Earth Planet. Sci. Lett., 200, 357–369, https://doi.org/10.1016/S0012-821X(02)00641-6, 2002.

Heyman, J., Applegate, P. J., Blomdin, R., Gribenski, N., Harbor, J. M., and Stroeven, A. P.: Boulder height - exposure age relationships from a global glacial $^{10}Be$ compilation, Quat. Geochronol., 34, 1–11, https://doi.org/10.1016/j.quageo.2016.03.002, 2016.

https://doi.org/10.5194/gchron-2024-34
Preprint. Discussion started: 9 December 2024


Hillebrand, T. R., Stone, J. O., Koutnik, M., King, C., Conway, H., Hall, B., Nichols, K., Goehring, B., and Gillespie, M. K.: Holocene thinning of Darwin and Hatherton glaciers, Antarctica, and implications for grounding-line retreat in the Ross Sea, 15, 3329–3354, https://doi.org/10.5194/tc-15-3329-2021, 2021.

Hippe, K.: Constraining processes of landscape change with combined in situ cosmogenic $^{14}C$-$^{10}Be$ analysis, Quat. Sci. Rev., 173, 1–19, https://doi.org/10.1016/j.quascirev.2017.07.020, 2017.

Hippe, K. and Lifton, N. A.: Calculating Isotope Ratios and Nuclide Concentrations for In Situ Cosmogenic $^{14}C$ Analyses, Radiocarbon, 56, 1167–1174, https://doi.org/10.2458/56.17917, 2014.

Hippe, K., Kober, F., Baur, H., Ruff, M., Wacker, L., and Wieler, R.: The current performance of the in situ $^{14}C$ extraction line at ETH, Quat. Geochronol., 4, 493–500, https://doi.org/10.1016/j.quageo.2009.06.001, 2009.

Hippe, K., Kober, F., Wacker, L., Fahrni, S. M., Ivy-Ochs, S., Akçar, N., Schlüchter, C., and Wieler, R.: An update on in situ cosmogenic $^{14}C$ analysis at ETH Zürich, Nucl. Instruments Methods Phys. Res. Sect. B Beam Interact. with Mater. Atoms, 294, 81–86, https://doi.org/10.1016/j.nimb.2012.06.020, 2013.

Hippe, K., Ivy-Ochs, S., Kober, F., Zasadni, J., Wieler, R., Wacker, L., Kubik, P. W., and Schlüchter, C.: Chronology of Lateglacial ice flow reorganization and deglaciation in the Gotthard Pass area, Central Swiss Alps, based on cosmogenic $^{10}Be$ and in situ $^{14}C$, Quat. Geochronol., 19, 14–26, https://doi.org/10.1016/j.quageo.2013.03.003, 2014.

Jeong, A., Il, J., Bae, Y., Balco, G., Yoo, K., Il, H., Domack, E., Hee, H., and Yong, B.: Late Quaternary deglacial history across the Larsen B embayment , Antarctica, Quat. Sci. Rev., 189, 134–148, https://doi.org/10.1016/j.quascirev.2018.04.011, 2018.

Johnson, J. S., Bentley, M. J., Smith, J. A., Finkel, R. C., Rood, D. H., Gohl, K., Balco, G., Larter, R. D., and Schaefer, J. M.: Rapid thinning of Pine Island glacier in the early Holocene, Science (80-. )., 343, 999–1001, https://doi.org/10.1126/science.1247385, 2014.

Johnson, J. S., Roberts, S. J., Rood, D. H., Pollard, D., Schaefer, J. M., Whitehouse, P. L., Ireland, L. C., Lamp, J. L., Goehring, B. M., Rand, C., and Smith, J. A.: Deglaciation of Pope Glacier implies widespread early Holocene ice sheet thinning in the Amundsen Sea sector of Antarctica, Earth Planet. Sci. Lett., 548, 116–501, https://doi.org/10.1016/j.epsl.2020.116501, 2020.

Johnson, J. S., Venturelli, R. A., Balco, G., Allen, C. S., Braddock, S., Campbell, S., Goehring, B. M., Hall, B. L., Neff, P. D., Nichols, K. A., Rood, D. H., Thomas, E. R., and Woodward, J.: Review article: Existing and potential evidence for Holocene grounding line retreat and readvance in Antarctica, 16, 1543–1562, https://doi.org/10.5194/TC-16-1543-2022, 2022.

Jones, A. G., Marcott, S. A., Gorin, A. L., Kennedy, T. M., Shakun, J. D., Goehring, B. M., Menounos, B., Clark, D. H., Romero, M., and Caffee, M. W.: Four North American glaciers advanced past their modern positions thousands of years apart in the Holocene, 17, 5459–5475, https://doi.org/10.5194/tc-17-5459-2023, 2023.

Jones, R. S., Johnson, J. S., Lin, Y., Mackintosh, A. N., Sefton, J. P., Smith, J. A., Thomas, E. R., and Whitehouse, P. L.: Stability of the Antarctic Ice Sheet during the pre-industrial Holocene, Nat. Rev. Earth Environ., 3, 500–515, https://doi.org/10.1038/s43017-

https://doi.org/10.5194/gchron-2024-34
Preprint. Discussion started: 9 December 2024


022-00309-5, 2022.

Jull, A. J. T., Scott, E. M., and Bierman, P.: The CRONUS-Earth inter-comparison for cosmogenic isotope analysis, Quat. Geochronol., 26, 3–10, https://doi.org/10.1016/j.quageo.2013.09.003, 2015.

Kingslake, J., Scherer, R. P., Albrecht, T., Coenen, J., Powell, R. D., Reese, R., Stansell, N. D., Tulaczyk, S., Wearing, M. G., and Whitehouse, P. L.: Extensive retreat and re-advance of the West Antarctic Ice Sheet during the Holocene, Nature, 558, 430–434, https://doi.org/10.1038/s41586-018-0208-x, 2018.

Koester, A. J. and Lifton, N. A.: Technical note: A software framework for calculating compositionally dependent in situ $^{14}$C production rates, 5, 21–33, https://doi.org/10.5194/gchron-5-21-2023, 2023.

Kohl, C. P. and Nishiizumi, K.: Chemical isolation of quartz for measurement of in-situ -produced cosmogenic nuclides, https://doi.org/10.1016/0016-7037(92)90401-4, 1 September 1992.

Lamp, J. L., Young, N. E., Koffman, T., Schimmelpfennig, I., Tuna, T., Bard, E., and Schaefer, J. M.: Update on the cosmogenic in situ $^{14}$C laboratory at the Lamont-Doherty Earth Observatory, Nucl. Instruments Methods Phys. Res. Sect. B Beam Interact. with Mater. Atoms, 456, 157–162, https://doi.org/10.1016/j.nimb.2019.05.064, 2019.

Lifton, N., Sato, T., and Dunai, T. J.: Scaling in situ cosmogenic nuclide production rates using analytical approximations to atmospheric cosmic-ray fluxes, Earth Planet. Sci. Lett., 386, 149–160, https://doi.org/10.1016/j.epsl.2013.10.052, 2014.

Lifton, N., Caffee, M., Finkel, R., Marrero, S., Nishiizumi, K., Phillips, F. M., Goehring, B., Gosse, J., Stone, J., Schaefer, J., Theriault, B., Jull, A. J. T., and Fifield, K.: In situ cosmogenic nuclide production rate calibration for the CRONUS-Earth project from lake Bonneville, Utah, shoreline features, Quat. Geochronol., 26, 56–69, https://doi.org/10.1016/j.quageo.2014.11.002, 2015a.

Lifton, N., Goehring, B., Wilson, J., Kubley, T., and Caffee, M.: Nuclear Instruments and Methods in Physics Research B Progress in automated extraction and purification of in situ from quartz : Results from the Purdue in situ 14 C laboratory, Nucl. Inst. Methods Phys. Res. B, 361, 381–386, https://doi.org/10.1016/j.nimb.2015.03.028, 2015b.

Lifton, N., Wilson, J., and Koester, A.: Technical note : Studying lithium metaborate fluxes and extraction protocols with a new , fully automated in situ cosmogenic $^{14}$C processing system at PRIME Lab, 5, 361–375, 2023.

Lifton, N. A.: A new extraction technique and production rate estimate for in situ cosmogenic carbon-14 in quartz, The University of Arizona, 1997.

Lifton, N. A., Jull, A. J. T., and Quade, J.: A new extraction technique and production rate estimate for in situ cosmognic $^{14}$C in quartz, Geochim. Cosmochim. Acta, 65, 1953–1969, https://doi.org/10.1016/S0016-7037(01)00566-X, 2001.

Longworth, B. E., Von Reden, K. F., Long, P., and Roberts, M. L.: A high output, large acceptance injector for the NOSAMS Tandetron AMS system, Nucl. Instruments Methods Phys. Res. Sect. B Beam Interact. with Mater. Atoms, 361, 211–216, https://doi.org/10.1016/j.nimb.2015.04.005, 2015.

https://doi.org/10.5194/gchron-2024-34
Preprint. Discussion started: 9 December 2024


Lupker, M., Hippe, K., Wacker, L., Kober, F., Maden, C., Braucher, R., Bourlès, D., Romani, J. R. V., and Wieler, R.: Depth-dependence of the production rate of in situ $^{14}C$ in quartz from the Leymon High core, Spain, Quat. Geochronol., 28, 80–87, https://doi.org/10.1016/j.quageo.2015.04.004, 2015.

Lupker, M., Hippe, K., Wacker, L., Steinemann, O., Tikhomirov, D., Maden, C., Haghipour, N., and Synal, H. A.: In-situ cosmogenic $^{14}C$ analysis at ETH Zürich: Characterization and performance of a new extraction system, Nucl. Instruments Methods Phys. Res. Sect. B Beam Interact. with Mater. Atoms, 457, 30–36, https://doi.org/10.1016/J.NIMB.2019.07.028, 2019.

Mackintosh, A., White, D., Fink, D., Gore, D. B., Pickard, J., and Fanning, P. C.: Exposure ages from mountain dipsticsk in Mac. Robertson Land, East Antarctica, indicate little change in ice-sheet thickness since the Last Glacial Maximum, Geology, 35, 551–554, https://doi.org/10.1130/G23503A.1, 2007.

Marrero, S. M., Phillips, F. M., Borchers, B., Lifton, N., Aumer, R., and Balco, G.: Cosmogenic nuclide systematics and the CRONUScalc program, Quat. Geochronol., 31, 160–187, https://doi.org/10.1016/j.quageo.2015.09.005, 2016.

Merchel, S., Bremser, W., Akhmadaliev, S., Arnold, M., Aumaître, G., Bourlès, D. L., Braucher, R., Caffee, M., Christl, M., Fifield, L. K., Finkel, R. C., Freeman, S. P. H. T., Ruiz-Gómez, A., Kubik, P. W., Martschini, M., Rood, D. H., Tims, S. G., Wallner, A., Wilcken, K. M., and Xu, S.: Quality assurance in accelerator mass spectrometry: Results from an international round-robin exercise for $^{10}Be$, Nucl. Instruments Methods Phys. Res. Sect. B Beam Interact. with Mater. Atoms, 289, 68–73, https://doi.org/10.1016/j.nimb.2012.07.038, 2012.

Milillo, P., Rignot, E., Rizzoli, P., Scheuchl, B., Mouginot, J., Bueso-Bello, J. L., Prats-Iraola, P., and Dini, L.: Rapid glacier retreat rates observed in West Antarctica, Nat. Geosci., 15, 48–53, https://doi.org/10.1038/S41561-021-00877-Z, 2022.

Mouginot, J., Scheuchl, B., and Rignot, E.: Mapping of Ice Motion in Antarctica Using Synthetic-Aperture Radar Data, Remote Sens., 4, 2753–2767, https://doi.org/10.3390/rs4092753, 2012.

Mouginot, J., Rignot, E., Scheuchl, B., and Millan, R.: Comprehensive annual ice sheet velocity mapping using Landsat-8, Sentinel-1, and RADARSAT-2 data, Remote Sens., 9, 1–20, https://doi.org/10.3390/rs9040364, 2017.

Nichols, K. A. and Goehring, B. M.: Isolation of quartz for cosmogenic in situ $^{14}C$ analysis, 1, 43–52, https://doi.org/10.5194/gchron-2019-7, 2019.

Nichols, K. A., Goehring, B. M., Balco, G., Johnson, J. S., Hein, A. S., and Todd, C.: New Last Glacial Maximum ice thickness constraints for the Weddell Sea Embayment, Antarctica, Cryosph., 13, 2935–2951, https://doi.org/10.5194/tc-13-2935-2019, 2019.

Phillips, F. M., Argento, D. C., Balco, G., Caffee, M. W., Clem, J., Dunai, T. J., Finkel, R., Goehring, B., Gosse, J. C., Hudson, A. M., Jull, A. J. T., Kelly, M. A., Kurz, M., Lal, D., Lifton, N., Marrero, S. M., Nishiizumi, K., Reedy, R. C., Schaefer, J., Stone, J. O. H., Swanson, T., and Zreda, M. G.: The CRONUS-Earth Project: A synthesis, Quat. Geochronol., 31, 119–154, https://doi.org/10.1016/j.quageo.2015.09.006, 2016a.

Phillips, F. M., Argento, D. C., Bourlès, D. L., Caffee, M. W., Dunai, T. J., Goehring, B., Gosse, J. C., Hudson, A. M., Jull, A. J.

https://doi.org/10.5194/gchron-2024-34
Preprint. Discussion started: 9 December 2024


T., Kelly, M., Lifton, N., Marrero, S. M., Nishiizumi, K., Reedy, R. C., and Stone, J. O. H.: Where now? Reflections on future directions for cosmogenic nuclide research from the CRONUS Projects, Quat. Geochronol., 31, 155–159, https://doi.org/10.1016/j.quageo.2015.04.010, 2016b.

Pigati, J. S., Lifton, N. A., Timothy Jull, A. J., and Quade, J.: A simplified In Situ cosmogenic $^{14}C$ extraction system, Radiocarbon, 52, 1236–1243, https://doi.org/10.1017/S0033822200046324, 2010.

Putnam, A. E., Schaefer, J. M., Barrell, D. J. A., Vandergoes, M., Denton, G. H., Kaplan, M. R., Finkel, R. C., Schwartz, R., Goehring, B. M., and Kelley, S. E.: In situ cosmogenic 10Be production-rate calibration from the Southern Alps, New Zealand, Quat. Geochronol., 5, 392–409, https://doi.org/10.1016/j.quageo.2009.12.001, 2010.

Rand, C. and Goehring, B. M.: The distribution and magnitude of subglacial erosion on millennial timescales at Engabreen , Norway, Ann. Glaciol., 1–9, 2019.

Rignot, E., Mouginot, J., and Scheuchl, B.: Antarctic grounding line mapping from differential satellite radar interferometry, Geophys. Res. Lett., 38, 1–6, https://doi.org/10.1029/2011GL047109, 2011a.

Rignot, E., Mouginot, J., and Scheuchl, B.: Ice flow of the antarctic ice sheet, Science (80-. )., 333, 1427–1430, https://doi.org/10.1126/science.1208336, 2011b.

Roberts, M. L., Burton, J. R., Elder, K. L., Longworth, B. E., McIntyre, C. P., von Reden, K. F., Han, B. X., Rosenheim, B. E., Jenkins, W, J., Galutschek, E., and McNichol, A. P.: A high performance $^{14}C$ Accelerator Mass Spectrometry System, Radiocarbon, 52, 228–235, 2010.

Rood, D. H., Hall, S., Guilderson, T. P., Finkel, R. C., and Brown, T. A.: Challenges and opportunities in high-precision Be-10 measurements at CAMS, Nucl. Instruments Methods Phys. Res. Sect. B Beam Interact. with Mater. Atoms, 268, 730–732, https://doi.org/10.1016/j.nimb.2009.10.016, 2010.

Rood, D. H., Brown, T. A., Finkel, R. C., and Guilderson, T. P.: Poisson and non-Poisson uncertainty estimations of $^{10}Be/\ ^{9}Be$ measurements at LLNL-CAMS, Nucl. Instruments Methods Phys. Res. Sect. B Beam Interact. with Mater. Atoms, 294, 426–429, https://doi.org/10.1016/j.nimb.2012.08.039, 2013.

Sbarra, C. M., Briner, J. P., Graham, B. L., Poinar, K., Thomas, E. K., and Young, N. E.: Evidence for a more extensive Greenland Ice Sheet in southwestern Greenland during the Last Glacial Maximum, 18, 1316–1329, https://doi.org/10.1130/GES02432.1, 2022.

Schimmelpfennig, I., Schaefer, J. M., Goehring, B. M., Lifton, N., Putnam, A. E., and Barrell, D. J. A.: Calibration of the in situ cosmogenic 14C production rate in New Zealand's Southern Alps, J. Quat. Sci., 27, 671–674, https://doi.org/10.1002/jqs.2566, 2012.

Scott, E. M., Naysmith, P., and Cook, G. T.: Should Archaeologists Care about $^{14}C$ Intercomparisons? Why? A Summary Report on SIRI, Radiocarbon, 59, 1589–1596, https://doi.org/10.1017/RDC.2017.12, 2017.

https://doi.org/10.5194/gchron-2024-34
Preprint. Discussion started: 9 December 2024


Slota, P. J., Jull, T. A. J., Linick, T. W., and Toolin, L. J.: Preparation of small samples for $^{14}C$ accelerator targets by catalytic reduction of CO, Radiocarbon, 29, 303–306, https://doi.org/https://doi.org/10.1017/S0033822200056988, 1987.

Søndergaard, A. S., Larsen, N. K., Steinemann, O., Olsen, J., Funder, S., Egholm, D. L., and Kjær, K. H.: Glacial history of Inglefield Land , north Greenland from combined in situ $^{10}Be$ and $^{14}C$ exposure dating, Clim. Past, 16, 1999–2015, 2020.

Spector, P., Stone, J., Cowdery, S. G., Hall, B., Conway, H., and Bromley, G.: Rapid early-Holocene deglaciation in the Ross Sea, Antarctica, Geophys. Res. Lett., 44, 7817–7825, https://doi.org/10.1002/2017GL074216, 2017.

Spector, P., Stone, J., and Goehring, B.: Thickness of the divide and flank of the West Antarctic Ice Sheet through the last deglaciation, 13, 3061–3075, https://doi.org/10.5194/tc-13-3061-2019, 2019.

Stone, J. O., Balco, G. A., Sugden, D. E., Caffee, M. W., Sass, L. C., Cowdery, S. G., and Siddoway, C.: Holocene deglaciation of Marie Byrd Land, West Antarctica, Science (80-. )., 299, 99–102, https://doi.org/10.1126/science.1077998, 2003.

Stutz, J., Mackintosh, A., Norton, K., Whitmore, R., Baroni, C., Jamieson, S. S. R., Jones, R. S., Balco, G., Salvatore, M. C., Casale, S., Lee, J. Il, Seong, Y. B., Mckay, R., Vargo, L. J., Lowry, D., Spector, P., Christl, M., and Ochs, S. I.: Mid-Holocene thinning of David Glacier , Antarctica : chronology and controls, Cryosph., 15, 5447–5471, 2021.

Venturelli, R. A., Siegfried, M. R., Roush, K. A., Li, W., Burnett, J., Zook, R., Fricker, H. A., Priscu, J. C., Leventer, A., and Rosenheim, B. E.: Mid-Holocene Grounding Line Retreat and Readvance at Whillans Ice Stream, West Antarctica, Geophys. Res. Lett., 47, https://doi.org/10.1029/2020GL088476, 2020.

Venturelli, R. A., Boehman, B., Davis, C., Hawkings, J. R., Johnston, S. E., Gustafson, C. D., Michaud, A. B., Mosbeux, C., Siegfried, M. R., Vick-Majors, T. J., Galy, V., Spencer, R. G. M., Warny, S., Christner, B. C., Fricker, H. A., Harwood, D. M., Leventer, A., Priscu, J. C., and Rosenheim, B. E.: Constraints on the Timing and Extent of Deglacial Grounding Line Retreat in West Antarctica, AGU Adv., 4, 1–15, https://doi.org/10.1029/2022AV000846, 2023.

White, D., Fülöp, R. H., Bishop, P., Mackintosh, A., and Cook, G.: Can in-situ cosmogenic $^{14}C$ be used to assess the influence of clast recycling on exposure dating of ice retreat in Antarctica?, Quat. Geochronol., 6, 289–294, https://doi.org/10.1016/j.quageo.2011.03.004, 2011.

Wilcken, K. M., Codilean, A. T., Fülöp, R. H., Kotevski, S., Rood, A. H., Rood, D. H., Seal, A. J., and Simon, K.: Technical note: Accelerator mass spectrometry of 10Be and 26Al at low nuclide concentrations, 4, 339–352, https://doi.org/10.5194/gchron-4-339-2022, 2022.

Young, N. E., Schaefer, J. M., Briner, J. P., and Goehring, B. M.: A $^{10}Be$ production-rate calibration for the Arctic, J. Quat. Sci., 28, 515–526, https://doi.org/10.1002/jqs.2642, 2013.

Young, N. E., Schaefer, J. M., Goehring, B., Lifton, N., Schimmelpfennig, I., and Briner, J. P.: West Greenland and global in situ 14C production-rate calibrations, J. Quat. Sci., 29, 401–406, https://doi.org/10.1002/jqs.2717, 2014.

https://doi.org/10.5194/gchron-2024-34
Preprint. Discussion started: 9 December 2024


Young, N. E., Lesnek, A. J., Cuzzone, J. K., Briner, J. P., Badgeley, J. A., Balter-Kennedy, A., Graham, B. L., Cluett, A., Lamp, J. L., Schwartz, R., Tuna, T., Bard, E., Caffee, M. W., Zimmerman, S. R. H., and Schaefer, J. M.: In situ cosmogenic $^{10}$Be-$^{14}$C-$^{26}$Al measurements from recently deglaciated bedrock as a new tool to decipher changes in Greenland Ice Sheet size, Clim. Past, 17, 419–450, https://doi.org/10.5194/cp-17-419-2021, 2021.